

COLD DARK CLOUDS: The Initial Conditions for Star Formation

EDWIN A. BERGIN

Department of Astronomy, University of Michigan, 500 Church St. Ann Arbor, MI, 48109, USA; email: ebergin@umich.edu

MARIO TAFALLA

Observatorio Astronómico Nacional, Alfonso XII 3, E-28014 Madrid, Spain; email: m.tafalla@oan.es

Key Words interstellar medium, interstellar molecules, molecular clouds, pre-stellar cores, star formation

Abstract Cold dark clouds are nearby members of the densest and coldest phase in the galactic interstellar medium, and represent the most accessible sites where stars like our Sun are currently being born. In this review we discuss recent progress in their study, including the newly discovered infrared dark clouds that are likely precursors to stellar clusters. At large scales, dark clouds present filamentary mass distributions with motions dominated by supersonic turbulence. At small, sub-parsec scales, a population of subsonic starless cores provides a unique glimpse of the conditions prior to stellar birth. Recent studies of starless cores reveal a combination of simple physical properties together with a complex chemical structure dominated by the freeze-out of molecules onto cold dust grains. Elucidating this combined structure is both an observational and theoretical challenge whose solution will bring us closer to understanding how molecular gas condenses to form stars.

CONTENTS

INTRODUCTION: HOLES IN THE HEAVENS	2
LARGE SCALE STRUCTURE OF COLD DARK CLOUDS	3
<i>Recent Studies</i>	3
<i>Observational Properties of Dark Clouds</i>	5
<i>Shapes</i>	6
<i>Mass Distribution</i>	6
<i>Velocity Structure</i>	7
<i>Internal Structure</i>	9
<i>Magnetic Field</i>	12
<i>Equilibrium State and Star Formation</i>	14
PHYSICS OF PRE-STELLAR MOLECULAR CORES	16
<i>Density</i>	17
<i>Temperature</i>	19
<i>Velocity Structure</i>	22
<i>Magnetic Field</i>	24

CHEMISTRY OF PRE-STELLAR MOLECULAR CORES	25
<i>Background</i>	25
<i>Observational Chemistry</i>	26
<i>Chemical Theory</i>	28
<i>Deuterium Chemistry and the Ionization Fraction</i>	30
<i>Key Tracers and the Possibility of Complete Heavy Element Depletion</i>	33
INFRARED DARK CLOUDS	33
<i>Background</i>	33
<i>Physical Properties and Implications</i>	34
SUMMARY AND FUTURE PROSPECTUS	35

1 INTRODUCTION: HOLES IN THE HEAVENS

“Hier ist wahrhaftig ein Loch im Himmel!” or “Here is truly a hole in the heavens!”, William Herschel was heard by his sister Caroline to exclaim in 1784 when he pointed his telescope towards the constellation Scorpius and viewed the dark nebulae in Ophiuchus (Houghton 1942). Herschel reported his discovery the following year (Herschel 1785), and for the next century astronomers debated whether these dark objects were truly voids, left by the stars as theorized by Herschel, or were perhaps nebulous dark regions observed projected upon a dense and bright stellar background. Our views began to change when Edward Emerson Barnard, who was motivated by Herschel’s discovery, published the first modern and systematic photographic survey of the “Dark Markings of the Sky” (Barnard 1919). Barnard argued that his deep photographs provided increasing evidence that many of these dark areas were “obscuring bodies nearer to us than the distant stars.”

Such regions might remain just obscured curiosities were it not for the clear association with star formation which began to be recognized in the mid-point of the twentieth century. The first person to do so was Bart J. Bok in 1946 (Bok 1948) when he claimed that the dark nebula, in particular compact and nearly round ones that now bear the name “Bok Globules”, are the sites of stellar birth. It was the advent of modern infrared and millimeter-wave technology in the latter half of the twentieth century that cemented the relation between Dark Clouds and the formation of stars and planetary systems.

The discovery of molecules in space further revealed that Dark Clouds are made of molecular material with H_2 as the dominant constituent (Weinreb et al. 1963; Wilson et al. 1970). Since this finding, the terms Molecular Cloud and Dark Cloud are often used interchangeably, as they refer to the two main characteristics of the clouds: their molecular composition and their opaque optical appearance. Molecular clouds are dark not because of their hydrogen molecules, but because of a population of tiny solids (“dust grains”) that absorb the optical starlight and lead to high visual extinctions ($A_V > 1^m$). Such a dimming of the starlight reduces the heating effects from external radiation and results in temperatures a few degrees above the 2.7 K cosmic background ($T \sim 10$ K).

For the purpose of this review we will use the term Cold Dark Cloud to refer to those molecular clouds that are close enough (< 500 pc) to be seen in silhouette against the background galactic starlight. These clouds (e.g. Taurus, Perseus, Ophiuchus, Lupus, ...) are observed to be forming low mass stars either in isolation or in small compact groups and have gas temperatures $\sim 10 - 20$ K. This

stands in contrast to diffuse clouds in the Milky Way, which contain molecular material but are not forming stars and are not optically opaque with $A_V \lesssim 1^m$. At the other end of the spectrum of galactic star formation lie the more distant and more massive Giant Molecular Clouds that form rich stellar clusters and contain embedded massive stars that heat the surrounding gas to temperatures > 20 K.

Over the past decade the development of sensitive continuum and heterodyne detectors at millimeter and sub-millimeter wavelengths has led to clear and important advances in our knowledge of the physics and chemistry of these Cold Dark Clouds. Particular progress has been made in the study of regions prior to onset of star formation, which is the primary focus of this review. We will first discuss the gains in our knowledge starting from the larger tens to hundreds of parsec scale of molecular clouds. We will follow with a detailed discussion of the physics and chemistry of the much smaller, ~ 0.1 pc, scale of molecular cloud cores, where recent research has clarified a number of outstanding issues. We conclude with a discussion of a newly discovered class of cold ($T_{\text{gas}} \sim 10 - 20$ K) dark clouds: infrared dark clouds that represent a new population of dense molecular regions and are believed to be the precursors to stellar clusters and massive stars.

Space constraints prohibit this review from complete coverage of the formation of clouds, stars, and planets. For more details we refer the reader to recent reviews of star formation (Larson 2003) (see also the review chapter by McKee and Ostriker, this volume), the role of turbulence (Mac Low & Klessen 2004; Elmegreen & Scalo 2004), probes of physical conditions (Evans 1999), gas/dust chemistry and star formation (van Dishoeck and Blake 1998; Ehrenfreund and Charnley 2000; van Dishoeck 2004), and the entire Protostars and Planets V volume (Reipurth et al. 2007), especially the papers by Ceccarelli et al., Di Francesco et al., and Ward-Thompson et al. that contain complementary reviews of this topic and include references that for reasons of limited space could not be mentioned here. Recent accounts of how the new observations with the Spitzer Space Telescope are advancing our knowledge of star formation in dark clouds can be found in Werner et al. (2006) and Allen et al. (2007).

While recent progress clearly warrants this review, the year 2007 presents an auspicious occasion for an overview of dark clouds. It is 150 years since the birth of E. E. Barnard in Nashville in December 1857, 101 years since the birth of B. J. Bok in the Netherlands, and 80 years since Barnard's Photographic Atlas of Selected Regions of the Milky Way was published posthumously (Barnard 1927). It is also the centennial of Barnard's beautiful exposure of Taurus-Auriga, which is shown in Fig. 1. The hundred years that separate us from Barnard's picture of Taurus have brought us a wealth of knowledge on the physics and chemistry of these dark patches. As we will see in this review, however, dark clouds remain in some aspects as mysterious and fascinating as when Barnard pointed his camera to them.

2 LARGE SCALE STRUCTURE OF COLD DARK CLOUDS

2.1 Recent Studies

A number of technical developments over the last decade have rapidly increased our ability to study dark clouds. Large-scale digital images in the optical, in-

frared, and radio regimes have become available in a routine or quasi-routine basis, and their analysis allows studying degree-sized portions of the sky at arcminute or better resolution. In the following sections we review some of these developments ordered by wavelength, and we briefly discuss the analysis techniques used to exploit this new wealth of data. Thanks to this recent progress, the study of cloud structure is currently enjoying a new golden age.

2.1.1 OPTICAL AND IR DATA The Digitized Sky Survey (DSS) and the USNO Precision Measuring Machine project (USNO-PMM; Monet 1996) have provided multi-band, all-sky images at optical wavelengths with accurate calibration and registration. Using different techniques, these data can be processed automatically to create large-scale images of dark clouds. Cambr sy (1999) has used USNO-PMM data together with a star-counting method to produce extinction (A_V) maps of up to ~ 250 square degrees for 24 dark clouds including Taurus, Perseus, and Ophiuchus. He has used an automatic adaptive grid with a fixed number of stars per cell to avoid empty pixels and to achieve a maximum extinction of around $A_V \sim 7$. This adaptive cell method, however, degrades the angular resolution of the images from about 1 arcminute in the outer parts of the clouds to about 10 arcminutes in the most opaque areas. A similar star-counting technique, but with a fixed cell spacing, has been used by Dobashi et al. (2005) to make an atlas of dark clouds using DSS-I data. These authors identify 2448 dark clouds toward the galactic plane ($b \leq 40^\circ$) and present maps with angular resolutions of $6'$ and $18'$ that are publicly available (<http://darkclouds.term.jp>).

Near infrared observations can be used to extend the optical extinction measurements to the most opaque regions of clouds thanks to the wavelength dependence of the dust absorption. The recent development of large-format infrared arrays has made it possible to apply this technique to increasingly large regions of the sky, and thus complement the work carried out at optical wavelengths. In addition to applying the star-count method, which provides an estimate of the average extinction inside a grid cell, multi-band NIR observations can be used to provide a direct determination of the extinction towards individual background stars. This determination uses the small range of NIR colors spanned by the background stars (mostly giants), which for practical purposes and with little error can be assumed constant. The Near Infrared Color Excess (NICE) method of Lada et al. (1994) uses H and K observations of background stars together with an estimate of their intrinsic (H-K) color from a nearby unobscured control field to derive A_V for each observed star. As an application of this method, Lada et al. (1994) produced an accurate map of the extinction towards the IC 5146 dark cloud with a resolution of 1.5 arcminute (also Lada, Alves & Lada 1999). An improvement of this technique is the NICER (NICE Revisited) method of Lombardi & Alves (2001), which uses observations in additional NIR bands to reduce the variance of the A_V estimate. By applying this method to the Orion data of the all-sky 2MASS survey (Skrutskie et al. 2006), these authors show that it is possible to derive large-scale cloud structure with $5'$ resolution to a limiting extinction of $A_V \approx 0.5$ (better or comparable to optical star-count work and below the threshold for molecular CO formation). Future use of this technique with 8m class telescopes is expected to provide accurate extinction maps with two orders of magnitude dynamical range and a resolution better than $10''$ (Lombardi & Alves 2001).

2.1.2 RADIO DATA In parallel with the technical advances in NIR cameras, millimeter and submillimeter-wavelength bolometer arrays have grown in size and sensitivity over the last decade. Arrays like SCUBA on the JCMT, MAMBO on the IRAM 30m telescope, and Bolocam on the CSO have made it possible to map systematically the thermal emission of cold dust from dark clouds (e.g. Motte, André & Neri 1998; Johnstone et al. 2000; Enoch et al. 2006). In contrast with their NIR counterpart, however, millimeter (mm) and submillimeter (submm) observations of dark clouds are sensitive to a narrower range of dust temperatures and suffer from severe instrumental limitations. The need to chop the telescope between sky and reference positions filters out part of the large-scale emission, which is usually weak enough to be close to the detection limit of the array. This means that bolometer observations miss most of the extended emission from a cloud while they recover its full small-scale structure. The future SCUBA-2 array at the JCMT, with its expected thousand-fold increase in mapping speed and high sensitivity for extended emission, promises to revolutionize the field of dust continuum mapping of dark clouds.

Molecular-line observations, on the other hand, provide information about the gas component of clouds, in particular about their velocity structure, density, temperature, and chemical composition. These data are complementary to the dust extinction and emission measurements, and they are required to understand, among other issues, the equilibrium status and the chemical evolution of dark clouds. Progress in mm-line receiver technology over the last ten years has also improved our ability to map large areas of the sky with increasing angular and spectral detail. Low resolution ($\approx 10'$) CO imaging of the entire Milky Way has been carried out with the CfA 1.2m telescope (Dame, Hartmann & Thaddeus 2001), and systematic mapping of selected clouds at higher resolution ($\approx 2'$) has been performed in CO isotopologues with the NANTEN/Nagoya 4m telescope (e.g., Tachihara et al. 2002) and the KOSMA 3m telescope (e.g., Sun et al. 2006). The 32-beam SEQUOIA array (and its predecessor, the 15-beam QUARRY array), operating at 3mm on the FCRAO 14m telescope, have been used to make megapixel images with sub-arcminute resolution of nearby clouds like Taurus (Fig. 1 and Goldsmith et al. 2005) and further out regions like the Galactic Ring (Jackson et al. 2006) and the outer Galaxy (Heyer et al. 1998). This array has also provided line data for the Coordinated Molecular Probe Line Extinction and Thermal Emission (COMPLETE) project (Ridge et al. 2006), which has the goal of combining the different IR and radio techniques of dark cloud mapping to study a series of dark clouds common to the Spitzer Space Telescope Legacy Program “From Molecular Cores to Planet Forming Disks” (c2d, Evans et al. 2003). The potential of heterodyne arrays, however, has not been fully exploited yet because the reduced number of pixels in the receivers limits the large scale observations to the bright lines of CO isotopologues. Further progress in this technology is still crucial to our understanding of the large-scale physics and chemistry of dark clouds.

2.2 Observational Properties of Dark Clouds

The dark cloud data obtained using the new instrumentation complements a large body of previous work summarized in previous reviews like those by Goldsmith (1987), Lada, Strom & Myers (1993), and Myers (1995). These new data have helped greatly to refine our understanding of the dark cloud properties, although,

as we will see, a number of important uncertainties still remain. In the following sections, we review some of the basic properties of clouds with emphasis on recently clarified issues and general characteristics from an observational point of view, concluding with a brief review of the issues whose solution remains pending. Because of space limitations, we cannot do justice to all the excellent studies of individual clouds carried out with the optical, IR, and radio instrumentation discussed before.

2.3 Shapes

A simple inspection of dark cloud images obtained by any of the methods discussed previously reveals that clouds come in a variety of sizes and shapes. In general, dark clouds have highly irregular edges, and their overall appearance is filamentary and often wind-blown. The presence of long, well-defined filaments was emphasized already a century ago by Barnard (1907) when he noted, describing the Taurus plate of Fig. 1, that “among the most surprising things in connection with these nebula-filled holes are the vacant lanes that so frequently run from them for great distances.” Indeed, some of the filaments in Taurus can be followed for more than 4 degrees or 10 pc, and similarly thin and long structures can be seen in many other clouds like Ophiuchus, Lupus, and Orion both in optical plates (e.g., Schneider & Elmegreen 1979) and radio images (e.g., Bally et al. 1987; Johnstone & Bally 1999).

In many clouds including Taurus and Ophiuchus, the length of some filaments is comparable to the full extent of the cloud. Typically, a cloud contains two or three long filaments that are either parallel or converge at a low angle in a massive condensation that often contains an active cluster-forming site (Tachihara et al. 2002; Burkert & Hartmann 2004). The velocity field of some filaments, in addition, seems rather coherent (see Loren 1989, for a study of Ophiuchus). This combination of spatial length and velocity coherence for some of the filaments suggests that their presence is intrinsic to the cloud structure and not the result of later evolutionary factors like star-formation activity, which would produce a more chaotic, small-scale mass distribution. Dark clouds, therefore, seem to be born with a filamentary distribution of material that extends over a number of parsecs. As clouds evolve and form stars, the products of star formation inherit the filamentary distribution of the parental gas (Hartmann 2002).

2.4 Mass Distribution

Maps of dark clouds provide more than just information on shapes. Measurements of dust extinction or gas column density at each cloud position can be used to estimate the amount of material under different physical conditions, and in particular at different densities. In his extinction study of 24 dark clouds, Cambr  sy (1999) finds that most of them present a similar power-law relation between the mass enclosed in an iso-extinction contour and the extinction, although the A_V range of this optical study is restricted to $A_V \approx 1-5$. Despite this limitation, the measurements illustrate how most of the material in a cloud lies at relatively low extinctions, and it must therefore reside in the form of low density gas. Using more sensitive NIR extinction data, Alves, Lada & Lada (1999) find that only 25-30% of the total mass in the IC 5146 and L977 cloud lies at $A_V > 10$, while Cambr  sy et al. (2002) finds that this percentage is slightly more

than 10% for the North America Nebula. A much smaller value ($\sim 1\%$) has been recently reported for the Pipe Nebula, also from IR extinction measurements (Lombardi, Alves & Lada 2006, also Lada, Alves & Lombardi 2007). Similar low fractions of dense material are indicated by large-scale maps of dust emission in clouds actively forming stars. Johnstone, Di Francesco & Kirk (2004) and Young et al. (2006) find that only between 1 and 2% of the mass in the Ophiuchus cloud is associated with dense, submm continuum emission, and that this emission is only detected towards regions of extinction larger than 10-15 mag. This is illustrated in Figure 2, which shows the IR-extinction and submm-emission maps of Ophiuchus from Young et al. (2006).

A related measure of how the mass of a cloud is distributed among different regimes is the statistics of extinction values. Ridge et al. (2006) find log-normal distributions for the number of pixels as a function of extinction in both Perseus and Ophiuchus, a distribution that is in agreement with the expectation from turbulent models of cloud formation (Vazquez-Semadeni 1994; Ostriker, Stone & Gammie 2001). Lombardi, Alves & Lada (2006), in their study of the Pipe Nebula, find that while a lognormal distribution provides an approximate general fit to the data, the observed histogram has significantly more structure that can only be reproduced with additional components.

2.5 Velocity Structure

The presence of supersonic motions in dark clouds has been known since the first molecular-line studies revealed non-gaussian line shapes and velocity differences across clouds of the order of 1 km s^{-1} or more (sound speed is 0.2 km s^{-1} for 10 K gas). These motions are inferred to be turbulent from the lack of systematic patterns like rotation, expansion, or infall (e.g., Heiles & Katz 1976), and from the existence of a systematic power-law relation between the velocity dispersion inside a cloud σ and its physical size L ($\sigma(\text{km s}^{-1}) = 1.10 L(\text{pc})^{0.38}$, Larson 1981), which is reminiscent of the classical Kolmogorov law of (incompressible) turbulence. Understanding and characterizing these turbulent motions, which affect not just dark clouds but the whole interstellar medium at almost every scale, is a formidable task. In contrast with their laboratory counterparts, turbulent motions in the interstellar medium are supersonic, compressible, and likely of magnetohydrodynamical nature. A rich field of both analytic and numerical work has been developed to tackle this problem, and a review of its results exceeds the scope of this paper. We refer the reader to the excellent recent review by Elmegreen & Scalo (2004) for an in-depth view of interstellar turbulence, especially from a theoretical point of view, and for an extensive list of references. Here we will concentrate on the main observational results of recent studies of dark cloud kinematics.

When studying the kinematics of cloud gas, it is necessary to take into account its dependence on density. Models of supersonic turbulence show that the highest density gas moves slower than the low density material, as it arises from the convergence of flows (e.g., Padoan et al. 2001), and this velocity segregation seems to be present in clouds. The densest regime in a cloud corresponds to the dense cores, which are known to have very low levels of turbulence and subsonic internal motions (e.g., Myers 1983). Dense cores seem therefore to lie at the bottom of the hierarchy of cloud kinematics, and to represent structures dominated by the dissipation of turbulence (e.g. Goodman et al. 1998). In § 3 we will present a

more complete summary of the physical properties of dense cores, and defer the discussion of dense gas kinematics to that section.

The kinematics of the low density gas in dark clouds at the small scales typical of dense cores (~ 0.1 pc) has been studied in detail by Falgarone et al. (1998). These authors selected 3 regions in nearby clouds and mapped them in different CO isotopologues over several arcminutes (tenths of a parsec for the clouds distance) with the IRAM 30m telescope. Each selected region contains a starless dense core, although the CO emission is dominated by the more diffuse material because of optical depth and depletion effects (see § 4.2). Even at their limit of angular resolution (about 1700 AU), Falgarone et al. (1998) find unresolved velocity structure, especially at the highest speeds. This fastest gas appears as prominent wings in non-Gaussian CO spectra with velocities of about 1 km s^{-1} and has an extremely filamentary distribution with aspect ratios larger than about 5. In contrast with the dense (10^5 cm^{-3}), subsonic, gas in a core, the fast CO-emitting gas (with a density of a few 10^3 cm^{-3}) presents large shears and velocity dispersions at the smallest resolvable spatial scales. The small regions of high shear may represent locations of enhanced dissipation of turbulence (Pety & Falgarone 2003).

The large-scale distribution of turbulence in clouds has been studied by a number of authors using different techniques. In addition to the classical linewidth-size relation of Larson (1981), methods used to analyze cloud kinematics include the statistics of the centroid velocity fluctuations (Miesch, Scalo & Bally 1999), the spectral correlation function (SCF, Rosolowsky et al. 1999), the principal component analysis (PCA, Heyer & Schloerb 1997), and the velocity channel analysis (VCA, Lazarian & Pogosyan 2000). A common goal of these methods is to identify and extract from maps of molecular-line emission a number of statistical properties of the velocity field that can be compared with the expectations from analytic theory (like Kolmogorov's law) or from numerical simulations of hydrodynamic and magnetohydrodynamic turbulence (e.g., Ossenkopf & Mac Low 2002; Ballesteros-Paredes et al. 2007). Two main issues addressed by these studies are the way in which the turbulent energy is distributed between the different spatial scales (as described by the energy spectrum $E(k)$) and the nature of the driving agent (for more details, see Elmegreen & Scalo 2004).

A recent example of the above type of work is the principal component analysis of 23 fields of the FCRAO CO Outer Galaxy Survey by Brunt & Heyer (2002). Using these and additional data, Heyer & Brunt (2004) have found an almost universal power-law form for the energy spectrum of clouds, with very little cloud-to-cloud scatter (10-20%) not only in the power law index but in the normalization coefficient. Such little scatter would help explain the emergence of Larson's law when combining data from an ensemble of clouds (Larson 1981). By combining numerical simulations of supersonic turbulence with an analysis of the velocity line centroid, the linewidth-size relation, and the PCA determinations of turbulence properties, Brunt & Mac Low (2004) suggest that observations of line emission from clouds are best fitted by compressible, shock-dominated (Burgers) turbulence. They also suggest that either clouds are recently formed or they are continually driven on large scales. These suggestive results still need confirmation from the systematic observation of a large number of nearby clouds and from the realistic modeling of the combined effect of cloud kinematics, chemistry, and radiative transfer. The extreme complexity of turbulent motions in clouds, the diverse mechanisms likely involved in their driving and dissipation, and the

challenge of obtaining high-quality molecular-line data of whole clouds will surely keep challenging theorists and observers alike for a number of years.

2.6 Internal Structure

A common feature of dark clouds is that they show a partly hierarchical structure, with smaller subunits appearing within large ones when observed with increasing spatial resolution. To characterize this structure, two different approaches have been generally followed, depending on whether the discrete or the continuous nature of the structure is emphasized. In the first approach, the cloud is assumed to be composed of subunits, referred as clumps and defined as coherent regions in position-velocity space that may contain significant substructure (Williams, Blitz & McKee 2000) (see below and Table 1 for typical clump parameters). These clumps are identified from the data using an automatic clump-finding algorithm that simplifies the process and avoids human bias. The most popular algorithms in use are GAUSSCLUMPS, developed by Stutzki & Güsten (1990), and CLUMPFIND from Williams, de Geus & Blitz (1994). These algorithms follow different approaches to identify and characterize clumps, but they generally agree in the derived properties, especially in the intermediate and high mass end (Williams, de Geus & Blitz 1994). When they are applied, usually to CO isotopologue data, the spectrum of clump properties is found to follow a power law in the range for which the data are complete. The mass of the clumps, for example, commonly presents a distribution of the form $dN/dM \sim M^{-\alpha}$, where α lies in a narrow range between 1.4 and 1.8 for both dark clouds and GMCs (Blitz 1993; Kramer et al. 1998). As a reference, and in this form, we note that the initial mass function of stars follows a steeper power law with a slope of $\alpha = 2.35$ (Salpeter 1955). The clump distribution, therefore, contains most of the mass in massive clumps, while the stellar distribution has most of the mass in low-mass objects.

The second approach to characterize cloud structure assumes that the cloud is self-similar, at least over some range of scales, and applies the concepts of fractal geometry. In this geometry, the most characteristic parameter of an object is its fractal (or Hausdorff) dimension, which is in general a non integer number (Mandelbrot 1983). The boundary of a cloud, for example, has a fractal dimension D_p that can be estimated from the relation between the enclosed area (A) and the perimeter length (P): $P \sim A^{D_p/2}$ (Lovejoy 1982). For simple curves in a plane, like circles or ellipses, this area-perimeter relation gives the expected value of $D_p = 1$ for the dimension of a line. For highly fragmented or convoluted curves, the expression gives a value that is larger than 1 and that approaches 2 as the curve fills a larger fraction of the plane. Beech (1987) used the above area-perimeter relation for the optical boundary of 24 dark clouds and derived an average boundary dimension of 1.4, which suggests that clouds are fractal. Using a similar method for the iso-contours of a series of CO maps, Falgarone, Phillips & Walker (1991) have derived a boundary dimension $D_p = 1.36 \pm 0.02$ for the Taurus molecular cloud, almost the same value measured by Scalo (1990) from IRAS maps. Similar values for the fractal dimension have been obtained for the more diffuse cirrus clouds ($D_p = 1.3$, Bazell & Desert 1988) and even for the atmospheric clouds on Earth ($D_p = 1.35$, Lovejoy 1982). As these dimension estimates use plane-of-the-sky views or maps of the objects, they only provide the fractal dimension of the clouds projection. To infer the

intrinsic (volume) fractal dimension, the area-perimeter value is generally increased by 1 (Beech 1992), although this procedure may only provide a lower limit to the true dimension (Sánchez, Alfaro & Pérez 2005). With this assumption, the area-perimeter determinations imply a typical cloud fractal dimension of around $D = 2.4$.

The very different approaches of the clump-finding and fractal analysis would seem to suggest that the two methods provide contradictory views of the cloud internal structure. This is however not the case, as the power-law behavior found in the spectra of clump properties already suggests a scale-free structure consistent with a fractal geometry (Elmegreen & Falgarone 1996, also Stutzki et al. 1998). Indeed, Elmegreen & Falgarone (1996) show that it is possible to derive clump mass distribution functions as those found by the GAUSSCLUMPS and CLUMPFIND algorithms from fractal cloud models of (volume) dimension $D = 2.3 \pm 0.3$. In this view, the clump-finding algorithms identify the peaks of the fractal intensity distribution of a cloud. Due to the threshold imposed in the density or column density by the observations, a power-law spectrum of cloud sizes results, and this produces a power-law distribution of clump masses even if the gas density follows a lognormal distribution (Elmegreen 2002).

The self-similar behavior revealed by both the power-law clump decomposition and the fractal description seems to apply inside a given range of spatial scales. This range most likely represents the regime dominated by turbulent motions, as turbulence produces self-similar structures in a natural way (e.g., Elmegreen & Scalo 2004). At large scales, the presence of well-defined features like filaments or shells indicates a deviation from self similarity that is likely caused by the mechanisms responsible for the cloud formation (e.g., Elmegreen & Falgarone 1996).

At small scales, in the gravity-dominated regime, the self-similar picture is also expected to break down. No break point from self similarity has yet been found in the lower density gas, and Falgarone et al. (1998) report unresolved turbulent structures at scales as small as 0.02 pc from their study of the highest velocity gas in the Taurus molecular cloud (also Pety & Falgarone 2003). For the dense star-forming gas, on the other hand, Larson (1995) has inferred a break down of the self-similar behavior in the form of a discontinuity in the slope of the surface density of companions for young stars in Taurus. This break point divides the binary regime from the clustering regime, and it occurs approximately at a radius of 0.04 pc, which coincides with the Jeans length of the cloud. Such coincidence suggests that for scales smaller than this length, thermal pressure provides the dominant support against gravity, while for larger scales, turbulent and magnetic pressures are important (Larson 1995). Followup work by Simon (1997) shows similar break points in the density of stellar companions for Ophiuchus and the Orion Trapezium, although the scale-size of the break point does not follow the expected Jeans mass. A larger value for the break point in the self-similar behavior of Taurus has been proposed by Blitz & Williams (1997) based on ^{13}CO observations, although optical depth effects and molecular freeze out (section § 4.2) may have affected this estimate.

There is further evidence for a change in the structure of dark clouds at small scales. As mentioned before, the clump mass spectrum found from large-scale CO observations is relatively flat, and follows a power law of the form $dN/dM \sim M^{-\alpha}$ with $\alpha = 1.4\text{--}1.8$. The mass spectrum of millimeter/submillimeter dust continuum peaks, on the other hand, presents a steeper slope of $\alpha = 2.0\text{--}2.5$ for

Table 1: Properties of Dark Clouds, Clumps, and Cores

	Clouds ^a	Clumps ^b	Cores ^c
Mass (M_{\odot})	10^3 – 10^4	50–500	0.5–5
Size (pc)	2–15	0.3–3	0.03–0.2
Mean density (cm^{-3})	50–500	10^3 – 10^4	10^4 – 10^5
Velocity extent (km s^{-1})	2–5	0.3–3	0.1–0.3
Crossing time (Myr)	2–4	≈ 1	0.5–1
Gas temperature (K)	≈ 10	10–20	8–12
Examples	Taurus, Oph, Musca	B213, L1709	L1544, L1498, B68

^a Cloud masses and sizes from the extinction maps by Cambr  s (1999), velocities and temperatures from individual cloud CO studies

^b Clump properties from Loren (1989) (^{13}CO data) and Williams, de Geus & Blitz (1994) (CO data)

^c Core properties from Jijina, Myers & Adams (1999), Caselli et al. (2002a), Motte, Andr   & Neri (1998), and individual studies using NH_3 and N_2H^+

masses larger than about $1 M_{\odot}$ (Motte, Andr   & Neri 1998; Testi & Sargent 1998; Johnstone et al. 2000, 2001). This spectrum, which at least for the case of Ophiuchus flattens to about $\alpha = 1.5$ for lower masses (Motte, Andr   & Neri 1998; Johnstone et al. 2000), mimics the shape of the initial mass function (IMF) of stars (Salpeter 1955; Miller & Scalo 1979), in contrast with the clump mass spectrum. Such similarity to the IMF suggests that stellar masses may be determined by the same process that fragments the molecular gas at the smallest scales.

The above discontinuity in the slope α still needs confirmation with a single observational technique, as each side of the break point has been observed with a different tracer (CO for large scales and mm/submm continuum for small scales). If confirmed, the discontinuity will suggest a change in the physics of the cloud gas at the tenth of a parsec scale, and this can provide the basis for an empirical description of the different levels of cloud structure. Williams, Blitz & McKee (2000) have recently proposed one such a categorization of structure in terms of clouds, clumps, and cores, with clumps being defined (as before) by their velocity coherence and cores being defined as gravitationally bound, single peaked regions out of which individual stars (or simple stellar systems) form. Alternative definitions have already been proposed (e.g., Goldsmith 1987; Myers 1995), and it is also possible that any description of cloud structure using only a few elements is too simple to capture the continuous properties of cloud gas (Rodr  guez 2005). Still, the need to name and characterize the different levels in the hierarchical structure of clouds makes it necessary to have a well accepted terminology, and the categorization by Williams, Blitz & McKee (2000) matches the spirit of current usage. Thus, using this convention, we present in Table 1 a summary of the main physical parameters of clouds, clumps, and cores. We stress that these units are still loosely defined and that their properties may be sensitive to the tracer used in the measurement and can vary with cloud. Future improvements in our understanding of cloud chemistry and structure will help further refine the above description.

2.7 Magnetic Field

The magnetic field of a cloud is probably its most difficult property to measure. The line of sight strength of the field can only be directly determined observing the Zeeman splitting of line transitions, and its plane of the sky direction can be estimated via polarization measurements of background stars, dust emission, or spectral lines. All these measurements require observations that combine stability and high signal to noise, and are therefore difficult and time consuming (see Heiles et al. 1993 for an in depth review of observational techniques of magnetic field measurements). Although the magnetic field only acts directly on charged particles (electrons, ions, and charged dust grains), its presence can be felt by the neutral material through collisions. Under most dark cloud conditions, this ion-neutral coupling is highly efficient and, except for the densest regions, the field is expected to be frozen to the gas (see McKee et al. 1993 for a review of the basic magnetic field theory). Because of this, the ability of the magnetic field to counteract the action of self-gravity can be critical to the equilibrium balance of dark clouds.

The most straightforward way to map the large-scale orientation of the magnetic field in a cloud is to measure the polarization of light from background stars, which results from the dichroic extinction by aligned, elongated dust grains (e.g., Davis & Greenstein 1951). Large-scale maps of polarization for the Taurus cloud have been presented by Moneti et al. (1984) and Heyer et al. (1987). Goodman et al. (1990) have produced maps of the optical polarization for Perseus, Taurus, and Ophiuchus using a combination of their own measurements with previous data. From these maps, they find that in Taurus and Ophiuchus the pattern of polarization is highly regular over scales of about 10 pc, while the Perseus measurements seem to suffer from the superposition of two components along the line of sight. In Taurus and Ophiuchus, the large scale filaments are neither completely parallel nor completely perpendicular to the global polarization pattern, suggesting that the magnetic field does not dominate the cloud structure on large scales (Goodman et al. 1990). Optical polarization data from other clouds offer a mixed picture. Clouds generally present fields with a well-defined mean direction but significant dispersion (Myers & Goodman 1991), and cases where the field is parallel or perpendicular to a filament exist (e.g., the long filamentary Musca cloud presents an ordered field perpendicular to the long axis of the filament, see Pereyra & Magalhães 2004).

While optical polarization measurements are necessarily limited to the low-extinction parts of a cloud, so the background stars are still bright enough to have their polarization measured, IR polarization data could in principle sample more opaque regions and therefore provide a deeper view of the inner magnetic field. Unfortunately, this seems not to be always the case. For the Taurus cloud, for example, there is evidence that the dust loses its polarizing power at depths larger than about $A_V = 1.3$, so IR polarization measurements offer little improvement over optical data in this region (Goodman et al. 1995; Arce et al. 1998). This loss of polarizing power probably results from a combination of a change in the alignment properties of grains and a change in their optical properties because of coagulation and mantle growth, although the exact mechanism is not yet well understood (Lazarian, Goodman & Myers 1997; Whittet et al. 2001).

Better sampling of the innermost cloud regions is expected from polarization measurements of the millimeter/submillimeter emission from dust, although

they also suffer often from drops in polarizing power towards the densest areas (Matthews, Wilson & Fiege 2001). Because of limitations due to sensitivity and spatial filtering, large scale studies of the dust polarization have concentrated on the brightest objects like the Orion filament (Matthews & Wilson 2000; Houde et al. 2004) instead of the more nearby and colder dark clouds (see § 3.4 for submm-polarization studies of dense cores). As in the case of the optical/IR polarization measurements, the limited submm measurements do not show a very strong correlation between the magnetic field direction and the mass distribution in the clouds (e.g., Houde et al. 2004).

Zeeman effect observations of dark clouds provide an estimate of the strength of the (line of sight component of the) magnetic field. The high signal-to-noise required by these measurements and the low spatial resolution achieved, because of the low frequency of the transitions, means that no large-scale maps of Zeeman effect measurements are currently available. Observations are commonly restricted to single pointings, which offer only a limited sampling of the magnetic field strength in clouds. In addition, and due to the need for strong emission, the pointings tend to be selected towards the densest regions. Still, coming up with meaningful detections is challenging, and the OH Zeeman observations of dark clouds by Crutcher et al. (1993) produced one clear detection out of 12 positions observed (mostly in Taurus and Ophiuchus). These data, together with the observations of Troland et al. (1996) suggest typical magnetic field strengths of order of $10 \mu\text{G}$ or less.

A main issue for the studies of the magnetic field strength in cloud gas is the importance of the field in the dynamics and balance of the cloud. A convenient parameter to characterize this importance is the observed ratio between the mass and the magnetic flux normalized to the critical value $\alpha G^{-1/2}$, where G is the gravitational constant and $\alpha \sim 0.13$ (see McKee et al. 1993 for a full discussion and equations). If the observed mass-to-flux ratio exceeds the critical value, the cloud is said to be supercritical and the magnetic field cannot prevent collapse. If the ratio is lower than the critical value, the cloud is called subcritical and gravity is stabilized by the magnetic field. A detailed compilation and analysis of the currently available data on magnetic field strength in molecular clouds has been presented by Crutcher (1999), and an update of this work appears in the review by Heiles & Crutcher (2005). According to this analysis, the magnetic field strength is just at the level of being critical, i.e., at the boundary between being dynamically important and not. Even in this best-to-date analysis, there are important caveats due to the large number of non-detections and the need to correct geometrically the mass-to-flux ratio (multiplying by 2 in case of a sphere or by 3 in case of a sheet, see Bourke et al. 2001 and Heiles & Crutcher 2005). The values, in addition, are likely more representative of the densest regions than of the extended cloud gas although chemical effects may further complicate the interpretation (§ 4.2). Thus, despite the enormous observational effort, the dynamical importance of the magnetic field in clouds, especially at the large scales, remains elusive. The current best guess is that the magnetic field contributes in a non-negligible way to the energy balance of molecular clouds. Whether it is a dominant player or a second order effect cannot be decided yet, and because of this, our understanding of the global equilibrium of dark clouds is still incomplete.

2.8 Equilibrium State and Star Formation

The equilibrium state of dark clouds and the way they collapse under gravity to form stars is probably the most controversial issue related to their nature. The uncertainties in the magnetic field strength and the importance of the turbulent motions, together with a possible revision of the lifetimes of the molecular gas (e.g. Hartmann, Ballesteros-Paredes & Bergin 2001), have resulted in two opposed views of the global state of clouds. Briefly, one view holds that clouds are close to equilibrium and that their evolution toward star formation is approximately quasistatic. The other view defends that clouds are dynamic objects that evolve and form stars in a crossing time. The limited space of this review cannot make justice to the number of issues involved in this controversy or to the detailed position of each camp, which consists of a number of authors working often independently. Here we will simply review the main contentious points and mention a number of relevant references as an introduction to the topic. We refer the reader to the original papers and the reviews mentioned below for an in-depth view of the controversy.

The quasistatic view holds that clouds are objects close to equilibrium, due to their relatively long lives (at least 10 Myr according to the recent estimate by Mouschovias, Tassis & Kunz 2006, see also Blitz & Shu 1980) and their being gravitationally bound and close to virialized (e.g., Larson 1981; McKee 1999). In this view, the equilibrium against self gravity is provided by the magnetic field, which has a twofold contribution toward stability. If the static component of the magnetic field is strong enough to make the cloud subcritical, gravitational forces cannot overcome magnetic forces as long as the field remains frozen into the matter (Mestel & Spitzer 1956; Nakano & Nakamura 1978). Hydromagnetic waves, in addition, can provide additional support and contribute to the supersonic motions observed in molecular clouds (Arons & Max 1975; Gammie & Ostriker 1996). In this magnetically-dominated picture, molecular clouds can only evolve under gravity and form stars through the process of “ambipolar diffusion,” by which neutrals drift past the ions and the magnetic field, which remain frozen to each other. Through the action of ambipolar diffusion, cores of dense gas form by gravitational contraction out of the initially subcritical medium. When these cores have accumulated enough mass, they become supercritical and collapse to form stars (Mestel & Spitzer 1956; Shu, Adams & Lizano 1987; Mouschovias & Ciolek 1999). Under typical cloud conditions, ambipolar diffusion is slow (several cloud dynamical times, see § 4.3.2), and this slowness makes cloud evolution prior to star formation occur quasistatically. It also makes star formation a rather inefficient process, in agreement with the low rate of stellar birth observed in the Galaxy (Zuckerman & Evans 1974).

The more recent and opposite view of cloud evolution and star formation emphasizes the role of supersonic turbulence and lack of equilibrium. Numerical simulations have shown that magnetic turbulence decays in about a dynamical time (Mac Low et al. 1998; Stone, Ostriker & Gammie 1998; Padoan & Nordlund 1999), so hydromagnetic waves cannot provide support against gravity without a source of continuous replenishment. If in addition fields are weak enough so molecular clouds are supercritical (e.g., Nakano 1998), cloud evolution and star formation becomes a fast process that occurs in a crossing time (Elmegreen 2000). In this picture, clouds form from convergent flows, evolve, and dissipate rapidly, without ever reaching a state of equilibrium, and with a typical molecular cloud lifetime of

3-5 Myr (Ballesteros-Paredes, Vázquez-Semadeni & Scalo 1999; Hartmann, Ballesteros-Paredes & Bergin 2001; Vázquez-Semadeni, Ballesteros-Paredes & Klessen 2003; Hartmann 2003). Molecular clouds are defined observationally by the detection of CO emission (as opposed to H₂ emission) and this lifetime refers to the age of the CO emitting cloud, which is associated with star formation. Chemical models suggest that H₂ formation is a pre-requisite to CO formation (Bergin et al. 2004), and lifetime estimates do not include any earlier phase when gas is predominantly molecular (e.g. H₂) but CO has not formed in sufficient quantity for detectable emission. Factors such as ram pressure, molecule and dust shielding, and gas-grain physics influence the timescales for both H₂ and CO formation (Koyama & Inutsuka 2000; Bergin et al. 2004). But in any case, it is clear that substantial evolution ($\sim 10 - 20$ Myr) occurs in a pre-CO phase where the cold H I and H₂ would be difficult to detect (Bergin et al. 2004). Formation of cloud structure in this scenario is regulated by the stochastic action of turbulence, which produces strong density perturbations through its fluctuating velocity field. Regions of dense gas form at the stagnation point of two convergent flows (Padoan et al. 2001), although such a transient structure often disperses when the flows fade. If the initial compression is strong enough, it may decouple from the medium and produce a dense core that subsequently collapses to form stars. This process of creating structure through the interplay between gravity and turbulence is often referred as gravoturbulent fragmentation (e.g., Klessen & Ballesteros-Paredes 2004) and lies at the heart of the dynamic picture of star formation (see the reviews by Mac Low & Klessen 2004, Larson 2003, and Ballesteros-Paredes et al. 2007).

The controversy between the fast and slow modes of cloud evolution and star formation is still ongoing and far from settled. Attempts to determine cloud lifetimes using stellar ages, for example, have not only not clarified the issue but have led to their own controversy (e.g., Palla & Stahler 2002; Hartmann 2003). Chemical analysis of the gas can also provide an estimate of cloud timescales. Observations of cloud cores, for example, suggest compositions that are far from equilibrium and ages that are $\lesssim 3 \times 10^5$ yrs (e.g. Pratap et al. 1997; van Dishoeck and Blake 1998), although this chemical age might not reflect the true cloud age but rather refer to the last time the chemistry was reset by some dynamical event. Studies of cold H I in dark clouds, on the other hand, suggest longer timescales $> 3 \times 10^6$ yrs (Goldsmith & Li 2005). Measurements of the magnetic field, as mentioned before, remain ambiguous because the data populate the boundary between the critical and subcritical regimes (Crutcher 1999), and this is often interpreted as proof of the magnetic field being dominant or a minor player.

The above summary of the current controversy illustrates how our understanding of dark cloud physics is still limited and far from complete. The observations and theoretical work carried out over the last decade have clearly revitalized the field of cloud studies and challenged many ideas previously assumed correct. Unfortunately, they have not achieved yet a consensus view of how clouds form, evolve to form stars, and finally disperse. It is therefore a challenge left for the next generation of cloud studies to explain the diversity of observations and to develop a global view of clouds, from the large, tens-of-parsecs scale to the tenths-of-parsec size of the dense cores, to which we now will turn our attention.

3 PHYSICS OF PRE-STELLAR MOLECULAR CORES

Dense cores are localized density enhancements of the cloud material that have been recognized for more than 20 years as the likely sites of low-mass star formation in nearby dark clouds like Taurus and Perseus. Initial core studies, based on the optical inspection of the Palomar plates together with molecular (especially NH_3) observations, showed that dense cores have typical sizes of 0.1 pc and contain a few solar masses of subsonic material at temperatures around 10 K and average densities of a few 10^4 cm^{-3} (Myers & Benson 1983; Benson & Myers 1989). The correlation of dense core positions with the location of highly embedded young stellar objects (YSOs) detected with the IRAS Far-Infrared (FIR) satellite soon provided the proof that some dense cores are currently forming stars or have done so very recently (Beichman et al. 1986). The presence of an embedded YSO has also led to the classification of cores in two groups: starless and star-containing. Strictly speaking, the distinction between the groups is only based on the threshold for detection of an embedded YSO with current instrumentation, which was until recently of the order of $0.1 L_\odot$ for nearby clouds like Taurus (Myers et al. 1987). The increase in the sensitivity of IR observations brought by the Spitzer Space Telescope has led to the discovery of a number of so-called very low luminosity objects (VeLLOs) in a few previously-thought starless cores, forcing a revision of the core classification (e.g., L1014, see Young et al. 2004). Still, the distinction between starless and star-containing cores seems a fundamental one, as it likely represents the separation between the pre-stellar and post-stellar phases of core contraction. The study of starless cores, therefore, offers the best opportunity to determine the initial conditions of low-mass stellar birth.

Dark globules (often called Bok globules or Barnard objects) are classically defined by their optical appearance as small, roundish, and dark nebulosities (Bok & Reilly 1947). They constitute a less homogeneous class than the dense cores of dark clouds, as they span sizes up to about 1 pc and masses of up to almost $10^3 M_\odot$, and have lower average densities (Bok 1977). A number of small globules, however, shares many characteristics with the dense cores, and are also the formation sites of individual low-mass stars (Clemens & Barvainis 1988; Yun & Clemens 1990). These dense globules may have a similar formation mechanism as the dense cores, with the difference that globules do not lie embedded in a molecular cloud because they have been exposed by an external event (such as ionization from a nearby O star, Reipurth 1983). Like some dense cores, some globules seem starless and centrally concentrated, and probably represent a phase prior to gravitational collapse. As we will see below, their isolated nature provides an additional advantage when studying the internal structure of pre-stellar objects (Alves, Lada & Lada 2001).

The study of dense cores and globules prior to star formation has progressed enormously during the last decade. Earlier work lacked the angular resolution needed to study their internal structure, and it therefore concentrated on global properties like total masses and average densities (e.g., Benson & Myers 1989; Clemens & Barvainis 1988). The progressive increase in resolution and sensitivity of radio and IR observations has finally allowed a detailed view of their interior. Through a combination of techniques that trace the gas and dust components, a new understanding of their internal structure has started to emerge. Crucial to this understanding has been the realization that dense cores and globules,

despite their apparent simplicity, have a rather complex chemical composition that is responsible for previous contradictions between observations made with different tracers. In this section we review some of the recent results concerning the physical structure of starless cores and globules, and the following section does the same for their chemical properties. For the sake of economy, we will refer to both cores and globules simply as cores, and we will only make an explicit distinction between the two when necessary. We will also use the term “starless” in a broad sense that includes what in the literature is sometimes referred to as “pre-stellar.”

3.1 Density

The density structure of pre-stellar cores is typically estimated through the analysis of dust emission or absorption. Three main techniques have been used so far: (1) near-infrared extinction mapping of background starlight, (2) mapping of mm/submm dust continuum emission, and (3) mapping of dust absorption against the bright galactic mid-infrared background emission. Each technique uses dust observations to derive a parameter that is proportional to the gas column density, and then fits this parameter with a model density profile that assumes some simple geometry (usually spherical). Fig. 3 shows a summary of how each technique works, including maps of representative cores (B68, L1544, and ρ Oph D), the main equations used in the analysis, and the radial profiles of the dust-derived parameter to be fit with the density model.

Because of their different assumptions, the above techniques are sensitive in different ways to the properties of the dust and to the variation of these properties inside the core. Uncertainties in the dust parameters propagate in different manner and affect differently the final density determination of each technique. The NIR extinction method, for example, is independent of the dust temperature, but depends on the reddening law (using $r_v^{H,K}$ to convert A_K into A_V) and on the correlation between A_V and the gas column density, both of which may be variable (see Rieke & Lebofsky 1985 and Bohlin et al. 1978 for typical ISM values). The mm/submm dust continuum emission method, on the other hand, depends almost linearly on the dust temperature and on the value of the dust emissivity (κ_ν), two parameters that are known to vary systematically as a function of core depth (see 3.2.1 for more details). The mid-infrared absorption method is also subject to uncertainties. It is sensitive to fluctuations in the emission from polycyclic aromatic hydrocarbons (PAHs), which provides the bright background against which the core is observed. It also depends on the somewhat uncertain relation between the absorbing opacity and the hydrogen column density (see Weingartner & Draine 2001 and Ragan et al. 2006 for further details). Given the restricted use of each of these methods (due to their difficulty and data requirements), no systematic inter-comparison between them has been carried out so far. As shown below, the methods agree in the qualitative characteristics of the density profiles, but a quantitative comparison of the inferred densities is still seriously needed. Without this, we can only guess the relative uncertainties of our density determination; current wisdom suggests that they are in the factor-of-2 range.

A main characteristic of the density profiles derived with the above techniques is that they require a central flattening. Pioneering work by Ward-Thompson et al. (1994) showed that the radial profiles of submillimeter continuum emission for a

number of cores could not be fitted using single power-law density distributions (assuming a constant dust temperature). At least two power laws were needed to fit the data, and the inner power law was always flatter than the outer one, which was usually close to r^{-2} . Follow up work with higher sensitivity has confirmed these early results for an increasing number of objects, and it has shown that as a rule, the density gradient of a core is flatter than r^{-1} within radii smaller than 2500-5000 AU, and that the typical central density of a core is 10^5 - 10^6 cm^{-3} (André, Ward-Thompson & Motte 1996; Ward-Thompson, Motte & André 1999). Although a dust temperature drop toward the core center is expected from thermal equilibrium considerations (Evans et al. 2001), the effect seems not strong enough to explain alone the flattening found in the continuum data. Observations using extinction techniques, which are insensitive to temperature, also find that a central flattening of the density profile is needed to fit the data. Bacmann et al. (2000), for example, have modeled MIR ($7\mu\text{m}$) absorption profiles from a sample of nearby starless cores observed with ISOCAM, and they have found that a decrease in the slope of the density distribution is required to fit the emission in the central 4000-8000 AU. Alves, Lada & Lada (2001) have mapped in detail the NIR extinction from the B68 globule and achieved an almost perfect fit with an equilibrium isothermal (Bonnor-Ebert) density profile that has a central flattening within ~ 5000 AU. Density profiles comparable to those inferred from observations are shown in Fig. 4.

A number of density laws with central flattening have been used to fit the observations of dense cores. The dual power law used initially by Ward-Thompson et al. (1994) is illustrative of the need for inner flattening, but presents an unphysical discontinuity in the derivative that results in a pressure jump. A simple alternative is the softened power laws used by Tafalla et al. (2002), and a more physical model is the truncated isothermal (Bonnor-Ebert, BE) sphere (Ebert 1955; Bonnor 1956), that often (but not always) provides a good fit to the data. Examples of good BE fits include those to the extinction profiles of a number of Bok globules (Alves, Lada & Lada 2001; Kandori et al. 2005) and dense cores Bacmann et al. (2000). Other physical models, on the other hand, seem to be ruled out by these observations. The logotropic density profile of McLaughlin & Pudritz (1996) is too flat at large radii (r^{-1}) to fit most cores (Bacmann et al. 2000), while the Plummer-like profile (Whitworth & Ward-Thompson 2001) seems asymptotically too steep (r^{-4}). Less clear is the situation of magnetic field-dominated models. These models naturally produce equilibrium configurations with flattened density profiles and approximately r^{-2} power-law behavior at large radius (e.g., Mouschovias 1976; Tomisaka, Ikeuchi & Nakamura 1988; Lizano & Shu 1989). Bacmann et al. (2000) find that some of these configurations provide adequate fits to their data, but that they require magnetic fields of the order of 50-150 μG , significantly larger than commonly observed (§ 3.4). They also predict oblate geometries, which seems to contradict some observations (Myers et al. 1991).

The high quality of some BE fits raises the question of whether cores are truly isothermal spheres solely supported by thermal pressure and confined by an outer medium. Several lines of evidence suggest that although thermal pressure is an important ingredient in core structure, it is not the only one, and that cores are more complex entities than simple BE spheres. In the first place, cores are seldom spherical, but they appear in the sky as elliptical objects with axial ratios typically of 2:1 (Myers et al. 1991). Whether cores are prolate, oblate, or triaxial is still a

matter of some debate (Myers et al. 1991; Ryden 1996; Jones, Basu & Dubinski 2001), but the lack of spherical symmetry already suggests either the presence of a non symmetrical force component or the lack of perfect equilibrium. In addition, the observed density contrast between the core center and its edge often exceeds the maximum value of ≈ 14 allowed for stable BE spheres (Bacmann et al. 2000; Evans et al. 2001), and it seems unlikely that such an unstable configuration can be realized in nature if thermal pressure is the only balancing force. Finally, the pressure required by the BE fits usually exceed the thermal (plus subsonic non-thermal) pressure available from the gas by a factor of a few, again indicating the presence of an additional force component or the lack of equilibrium (Tafalla et al. 2004; Kirk, Ward-Thompson & André 2005).

The BE-like profiles found when fitting observations must therefore result from a more complex physics than just thermal hydrostatics. Indeed, Myers (2005) and Kandori et al. (2005) have shown that these profiles can be reproduced with a variety of geometries and even under early conditions of gravitational collapse. Even models of supersonic turbulence can produce density condensations that have in projection the appearance of BE profiles (Ballesteros-Paredes, Klessen & Vázquez-Semadeni 2003), but their expected velocity structure is inconsistent with the prevalence of subsonic cores in dark clouds like Taurus (e.g., Jijina, Myers & Adams 1999, Tafalla et al. 2007, in preparation). The ultimate origin of the observed core density profiles remains therefore unexplained.

3.2 Temperature

The kinetic temperature of the dust and the gas components in a core is regulated by the equilibrium between heating and cooling. At typical core densities ($> 10^4 \text{ cm}^{-3}$), the gas and dust start to couple thermally via collisions (e.g. Goldsmith & Langer 1978; Burke & Hollenbach 1983), and the two temperatures are expected to converge; whether they equalize or not depends in part on the exact density of the core and on the strength of the external radiation field (Galli, Walmsley & Gonçalves 2002). In this and the next sections we discuss recent progress in the determination of the dust and gas temperatures of cores. As the two temperatures are determined using different observational techniques and are therefore subject to different uncertainties, we separate their discussion. We start with the dust.

3.2.1 DUST TEMPERATURE The dust temperature is physically determined by the balance between the heating by the interstellar radiation field (ISRF) and the cooling by thermal radiation from the grains in the FIR (Mathis, Mezger & Panagia 1983). To estimate this temperature observationally, color measurements of the dust in the submm or FIR are commonly used, sometimes complemented with NIR extinction measurements. A major uncertainty in this work is our limited understanding of the optical properties of the dust and, in particular, the value of the dust emissivity and how it changes as a function of density. Theoretical models of dust evolution predict that as the density increases, the dust grains become coated with ice and coagulate to form fluffy aggregates, changing their emissivity in the process (Ossenkopf & Henning 1994). Determining dust temperatures from observations therefore implies resolving simultaneously for their optical properties, in particular the emissivity (κ) and its wavelength dependence (commonly parametrized as ν^β).

Large-scale studies of dust temperature show that the grains in starless cores

are colder than in the surrounding lower-density medium, as expected from the attenuation of the ISRF deep inside the cloud. From ISO FIR (170 and 200 μm) observations toward the vicinity of a number of dense cores, Ward-Thompson, André & Kirk (2002) found a prevalence of flat or decreasing temperature gradients with cloud temperatures of 15-20 K and core values of 10-12 K. Because of the 1 arcminute resolution of these observations (0.04 pc at the distance of Taurus), the core value represents only an average temperature over the densest gas. Also using low-resolution ISO data and a similar analysis, Tóth et al. (2004) and del Burgo & Laureijs (2005) have derived inward temperature gradients that reach central values of ≈ 12 K for a number of Taurus cores, while for the denser L183 core a value close to 8 K has been measured (Lehtinen et al. 2003; Pagani et al. 2003). These temperature estimates, however, ignore the effects of grain evolution and assume a constant dust emissivity, while observations are beginning to show that the emissivity does in fact vary. FIR observations of a filament in Taurus by the PRONAOS balloon-borne experiment suggest that at the highest densities, the population of smallest grains disappears and the submillimeter emissivity increases by a factor of about 3, as expected by models of dust coagulation into fluffy grains (Stepnik et al. 2003). These observations also suggest inner dust temperatures around 12 K, although the 3-arcminute resolution sets an important limitation.

The trend of decreasing dust temperature with depth observed in the large scale maps is expected to continue inside the dense cores, but the exact shape of the resulting gradient is still a matter of some uncertainty. Initial models by Evans et al. (2001) and Zucconi, Walmsley & Galli (2001) suggested sharp core edge-to-center drops in temperature of about a factor of 2 (an example is provided in Fig. 4). However, these models either assumed that cores are directly exposed to the ISRF (correct for Bok globules only), or use a simple attenuation law for cores that are embedded in clouds. André et al. (2003) and Stamatellos & Whitworth (2003) have argued that the effect of the surrounding cloud is to flatten the temperature gradient, so that at the center of an embedded core the gradient is less pronounced (see Stamatellos et al. 2004; Gonçalves, Galli & Walmsley 2004, for 2D and 3D radiative transfer models). Irrespective of the models, however, central dust temperatures close to 7-8 K are predicted for typical dense cores, with the exact value depending on the dust central density and the presence or not of a surrounding cloud.

From an observational point of view, possible gradients in the dust emissivity still limit our estimate of the temperature profiles. Kramer et al. (2003) have combined submm emission and NIR extinction data to study several starless cores in IC 5146. With an angular resolution of 30 arcseconds, these authors find that the dust temperature is typically 12 K and close to constant inside the cores, while the surrounding, lower extinction material has a higher value of about 20 K. They also find that the dust emissivity increases systematically by a factor of 4 between 20 and 12 K, consistent with models of dust evolution (e.g., Ossenkopf & Henning 1994). Using similar technique and angular resolution, Bianchi et al. (2003) have also found an emissivity gradient in the B68 globule, together with an outer dust temperature of 14 ± 2 K and an inner temperature drop of a factor of 1.5. Schnee & Goodman (2005), on the other hand, have studied the submm emission from TMC-1C with $14''$ resolution and found a central gradient in the submm color. As illustrated in Fig. 5, this color gradient can result from either a central temperature drop to about 7 K or a systematic

change in the dust emissivity index (or both). Clearly more data and modeling are needed to characterize the existing gradients in dust conditions inside dense cores. Future multiwavelength mapping in the FIR with the Herschel satellite offers the best hope to finally disentangle the changes in temperature and optical properties.

3.2.2 GAS TEMPERATURE Like the dust temperature, the temperature of the gas is determined by the balance between heating and cooling. For the lower density cloud gas, heating mostly occurs through ionization by cosmic rays, while the cooling is mainly due to line radiation from molecules, especially CO (Goldsmith & Langer 1978). At the high densities of cores (more than a few 10^4 cm^{-3}), gas-dust coupling via collisions becomes important, and this process will additionally heat or cool the gas depending on the difference between the gas and dust temperatures (Burke & Hollenbach 1983). Also at these densities, and at typical core temperatures, CO and other molecules start to disappear from the gas phase due to their freeze out onto the dust grains (§ 4.2), diminishing the ability of the gas to cool down via line radiation. The detailed study of thermal balance in dense cores by Goldsmith (2001) shows that the gas-dust coupling, together with the high efficiency of the dust radiative cooling, easily compensates the disappearance of molecular coolants, and keeps the temperature of the gas deep inside the core at rather low values, comparable to those of the dust component. At the lower-density core edges, the gas and dust are thermally decoupled and the gas becomes warmer than the dust due to photoelectric heating. The temperature difference between the two components depends on the strength of the external UV field (see Fig. 4).

Keeping the gas cold and at a close-to-uniform temperature has important implications for the mechanical equilibrium of cores, as the gas component is the main contributor to the thermal pressure. Galli, Walmsley & Gonçalves (2002) have studied the equilibrium structure of a pressure-supported dense core with a realistic treatment of the gas and dust cooling. Although the resulting gas temperature distribution is not exactly constant, its gradient is shallow enough to require for stability a density profile which is very close to the Bonnor-Ebert solution (see Fig. 4). Thus, if cores were supported by thermal pressure only, the BE model would be consistent with the internal thermodynamics.

To measure the temperature of the gas component in clouds and cores, the level excitation of simple molecules like CO and NH_3 is commonly used (Evans 1999). CO and its isotopologues have small dipole moments, so their lower energy levels thermalize at relatively low densities of the order of few 10^3 cm^{-3} (Spitzer 1978), typical of the extended gas in dark clouds. Temperatures derived using CO in regions with no star formation indicate gas temperatures of 10-15 K, with a possible increase towards the lower density gas near the cloud edges (Snell 1981). Temperatures for the denser gas in cores are better determined using the metastable inversion levels of ammonia (NH_3), which can be observed simultaneously at a wavelength of about 1.3 cm (Walmsley & Ungerechts 1983). NH_3 , in addition, appears to rise in abundance in the densest ($n_{\text{H}_2} > 10^4 \text{ cm}^{-3}$) regions (§ 4.2), so it tends to selectively trace dense core gas. Low angular resolution NH_3 observations of dense cores typically indicate gas temperatures of about 10 K with a rather narrow range of variation for clouds like Taurus, Perseus, and Ophiuchus (Myers 1983; Benson & Myers 1989; Jijina, Myers & Adams 1999). These low-resolution measurements represent core-wide averages of the temperature, and

are in reasonable agreement with the theoretical expectations mentioned before. Due to the relatively low angular resolution of the NH_3 observations (caused by the low frequency of the transitions), few studies of the radial dependence of the gas temperature inside dense cores have been made. Tafalla et al. (2004) have studied the temperature profiles of two Taurus-Auriga starless cores, L1498 and L1517B, using NH_3 observations with a resolution of $40''$ (0.027 pc). In both cores, the temperature remains constant over the central 0.1 pc with a value of about 10 K. Higher resolution NH_3 observations of the denser starless core L1544 seem to indicate a decrease of the gas temperature toward the innermost parts of the core (Crapsi et al. in preparation). For the starless Bok globule B68, on the other hand, Bergin et al. (2006) have found an opposite effect: while the inner core traced by NH_3 is at about 10 K, the surrounding layers, traced with CO isotopologues, are slightly cooler (7-8 K). This central warming may result from a weakening of the gas-dust coupling at the highest densities due to grain coagulation. Given this diversity of results, further observations of the temperature gradients inside dense cores are needed to clarify the origin of these significant, but relatively small (20%), temperature differences.

3.3 Velocity Structure

In contrast with the supersonic velocity fields characteristic of the clouds as a whole, dense cores have low velocity internal motions. Starless cores in clouds like Taurus, Perseus, and Ophiuchus systematically present spectra of core-tracing species (e.g., NH_3) that have close-to-thermal linewidths, even when observed at low angular resolution (Myers 1983; Jijina, Myers & Adams 1999). This indicates that the gas motions inside the cores are subsonic, either in the form of random turbulence or as part of more systematic global patterns (Fig. 6).

Despite the slow speeds involved, the internal motions of cores are in general complex, with no single element identified as dominant. The excess in linewidth over the thermal value has commonly been interpreted as resulting from turbulent motions, although as we will see below, other velocity patterns like infall could contribute to the line broadening. Even in this interpretation, turbulent motions, by being subsonic, contribute less to the gas pressure than the thermal component, so they represent a minor contribution to the core support (Myers 1983; Goodman et al. 1998; Caselli et al. 2002a; Lada et al. 2003; Tafalla et al. 2004). Studying the spatial distribution of turbulent motions in cores, Goodman et al. (1998) have found that they deviate from the linewidth-size relation seen at large scales (§ 2.5, Larson 1981). Instead, the non-thermal component of the NH_3 linewidth in a core is approximately constant inside a “coherence” radius of about 0.1 pc (see also Caselli et al. 2002a; Tafalla et al. 2004). This coherence radius is close to the 0.04 pc radius found to separate the binary and clustering regimes in Taurus and interpreted as the length-scale at which the cloud self-similar behavior breaks down (§ 2.5, Larson 1995). It is therefore tempting to suggest that the coherence radius is the scale at which turbulence loses its grip on cloud motions and allows the formation of thermally dominated cores.

A rotation components is expected in any object that forms by the gravitational contraction of galactic material (Spitzer 1978). From the study of the spatial changes in the velocity centroid of lines, however, it has been known for some time that dark clouds as a whole are not rotating rapidly (Heiles & Katz 1976; Arquilla & Goldsmith 1986). Observations of dense cores and globules reveal a

similar lack of fast rotation in the dense gas. Goodman et al. (1993) analyzed the rotation patterns of 43 dense cores as derived from observations of the $\text{NH}_3(1,1)$ line, and estimated that the typical ratio between rotational and gravitational energies is only 0.02. These authors also found no correlation between the rotational axis and the orientation of core elongation, which is again indicative of rotation being only a minor element in core support. From higher resolution N_2H^+ observations of an equivalent sample of cores, Caselli et al. (2002a) have derived similarly low values of the rotational energy, and found that the point-to-point velocity gradients inside the cores are much more complex than expected for simple solid-body rotation. Rotation is therefore only one of the ingredients of core kinematics.

The slow rotation rate of dense cores is in fact remarkable. Arquilla & Goldsmith (1986) and Goodman et al. (1993) have shown that the specific angular momentum j in a core or a cloud scales with its radius R approximately as $R^{1.6}$. Clouds of 1 pc radius have typical j values around $10^{23} \text{ cm}^2 \text{ s}^{-1}$, while typical cores (0.05 pc radius) have j values of about $10^{21} \text{ cm}^2 \text{ s}^{-1}$. If this trend of decreasing j reflects the evolution of specific angular momentum as the cloud gas undergoes contraction, an efficient mechanism of angular momentum removal is required to reproduce the observations, and in particular, to explain the low j values of cores. Magnetic coupling between the contracting gas and the lower density environment has been classically favored as the mechanism for transferring angular momentum from a contracting core to its surroundings (Mestel & Spitzer 1956; Mouschovias & Paleologou 1979), although an alternative interpretation in terms of gravoturbulent fragmentation has recently been proposed (Jappsen & Klessen 2004). The low j value of cores is in fact comparable to or slightly larger than the value inferred for protostellar envelopes, T Tauri disks, and wide binaries, suggesting that the later phase of gravitational contraction of the core occurs with almost constant angular momentum (Bodenheimer 1995). Of course, a final phase of angular momentum redistribution via disk transport or tidal interactions between stars is still needed to explain the low specific angular momentum found in individual T Tauri stars (e.g., Shu, Adams & Lizano 1987; Bodenheimer 1995; Larson 2002).

Inward motions can also contribute to the dense core kinematics. They are inferred from the observation of optically thick, self-absorbed lines of species like CS, H_2CO , or HCO^+ , in which low-excitation foreground gas absorbs part of the background emission. In a core with inward motions, the foreground gas moves toward the background, so the absorbing material is red-shifted with respect to the emitting layers. The resulting spectrum is a self-absorbed profile with a red-shifted dip and a relatively brighter blue peak (see CS J=3-2 in Fig. 6), a pattern often called an infall asymmetry (Leung & Brown 1977; Myers et al. 1996). In a starless core, this spectral feature has been first identified towards L1544, for which an average inward velocity of about 0.1 km s^{-1} was inferred (Myers et al. 1996; Tafalla et al. 1998; Williams et al. 1999; Caselli et al. 2002b). A follow up single-pointing survey of 220 starless cores by Lee, Myers & Tafalla (1999) has found a statistically significant over-abundance of inward motions with typical velocities of $0.05\text{-}0.1 \text{ km s}^{-1}$, indicating that subsonic contraction is a common feature of core kinematics (also Gregersen & Evans 2000). The spatial distribution of these motions is typically large, $0.05\text{-}0.15 \text{ pc}$, and comparable to the observed size of the cores (Tafalla et al. 1998; Lee, Myers & Tafalla 2001). Such a large extent could result either from the gravitational collapse of a

core having a centrally condensed initial state (Myers 2005) or be associated with the process of core condensation (see Myers, Evans & Ohashi 2000, for a review).

Additional velocity patterns have been proposed to explain the observations of molecular lines in different cores. Lada et al. (2003) have found an asymmetric velocity field with both inward and outward motions in the B68 globule, and they have interpreted it as resulting from small amplitude pulsations of the core outer layers. Such a pattern seems in fact consistent with the close to Bonnor-Ebert density structure found in this object (Keto et al. 2006). Tafalla et al. (2004) have proposed that residual internal motions in L1498 and L1517B may originate from asymmetric contraction, as the motions are correlated with asymmetries in the pattern of depletion of species like CO and CS. Finally, by comparing the velocity centroids of N_2H^+ and CO isotopologues in a sample of 42 cores, Walsh, Myers & Burton (2004) have concluded that the relative velocity between the dense cores and the ambient medium is low ($\leq 0.1 \text{ km s}^{-1}$). This implies that newly born stars are not expected to move appreciably from their natal cores.

3.4 Magnetic Field

Estimates of the magnetic field in starless cores are mainly obtained from Zeeman splitting measurements and from polarization observations of the mm/submm dust continuum. Zeeman measurements have the disadvantage of a low angular resolution and the use of tracers sensitive to molecular depletion, so they are prone to miss the densest part of the cores. On the other hand, they are unique because they provide a direct estimate of the strength of the (line of sight component of the) magnetic field, B_{los} . From OH Zeeman measurements of the L1544 core with the Arecibo telescope, Crutcher & Troland (2000) have estimated a line of sight strength of about $11 \mu\text{G}$ averaged over a beam of 3 arcmin (about 0.1 pc), in good agreement with the prediction from a previous model of ambipolar diffusion (Ciolek & Basu 2000). These observations, however, are more sensitive to the large-scale cloud gas than to the core material because of the the low dipole moment and the chemical distribution of the OH molecule in clouds (§ 4.2). Zeeman measurements using tracers of dense gas have mostly produced negative results, like $B_{los} \leq 100 \mu\text{G}$ in L1498 (CCS data, Levin et al. 2001) and $B_{los} \leq 15 \mu\text{G}$ in TMC-1 (C_4H data, Turner & Heiles 2006). Shinnaga, Tsuboi & Kasuga (1999), on the other hand, have reported an estimate of $160 \pm 42 \mu\text{G}$ in the young starless core L1521E from CCS observations.

Submm polarization measurements provide a direct estimate of the orientation of the (plane of the sky component of the) magnetic field. They can also be used to estimate indirectly the strength of the field by comparing the spatial dispersion of its orientation and the turbulence level of the gas (Chandrasekhar & Fermi 1953). As mentioned in § 2.7, these measurements often lose sensitivity towards the brightest, highest density regions, where the polarization fraction drops with intensity (Matthews & Wilson 2000; Henning et al. 2001; Wolf, Launhardt & Henning 2003), which again makes the estimates more sensitive to the field in the outer parts of the cores. Because of the combination of weak submm emission of the starless cores and a low polarization fraction ($\sim 10\%$), these observations are challenging and have only been carried out in a reduced number of objects. For cores L1544, L183, and L43, Ward-Thompson et al. (2000) and Crutcher et al. (2004) have found polarization vectors that are fairly uniform but not aligned with the minor axis of the cores by about 30° , as it would have been expected

by ambipolar diffusion models (but see Basu 2000 for an alternative view if the cores are triaxial). From the dispersion of the polarization vectors and the turbulence level of the gas, these authors estimate plane-of-the-sky intensities between 80 and 160 μG . Strictly speaking, these field intensities make the cores supercritical (i.e., with a magnetic field too weak to balance gravity). However, the inclusion of a geometrical correction factor moves the cores to the critical or slightly subcritical regime, suggesting that the field may be dynamically important (Crutcher et al. 2004). Lower field values of 10 and 30 μG have been estimated towards the cores L1498 and L1517B, respectively, indicating that these cores may be supercritical by factors of about 2 even after geometrical correction (Kirk, Ward-Thompson & Crutcher 2006).

As with the large scale magnetic field measurements (§ 2.7), the observations of cores provide an ambiguous answer to the question of whether magnetic fields dominate or not the equilibrium of dense cores. Clearly more observations of both the Zeeman effect and the dust polarization are needed to clarify the role of magnetic fields in the process of core and star formation. The close to critical values observed so far, however, suggest that unless observations have been systematically biased in one or the other direction, cores appear to be close to the point of criticality to within a factor of about 2. Explaining this apparent coincidence should therefore be a main requirement to any theory of core formation.

4 CHEMISTRY OF PRE-STELLAR MOLECULAR CORES

4.1 Background

The presence of gas phase chemical inhomogeneities within molecular clouds has been known for some time. In particular, spatial differences in emission morphologies between carbon chains (e.g. HC_3N , C_2S) and nitrogen-hydrogen molecules (NH_3 , N_2H^+) on scales of 0.05–0.2 pc were described (Suzuki et al. 1992; Pratap et al. 1997). Surveys of numerous cores in Taurus revealed larger emission sizes and velocity linewidths for CS when compared to NH_3 , despite similar line centroids (Zhou et al. 1989). These differences have generally been attributed to the slower timescales to activate the nitrogen chemistry as opposed to the carbon chemistry, or perhaps due to some dynamical cycling of material that can enhance the carbon chemistry (see van Dishoeck and Blake 1998; Langer et al. 2000, for a discussion of general chemistry).

In this regard two low-mass cores, TMC-1 and L134N, were isolated and studied as template objects because of their rich chemistry and due to the fact that they are unassociated with star formation activity (Swade 1989; Hirahara et al. 1992; Pratap et al. 1997). Over one thousand papers have been written for these two objects alone. In general chemical studies computed average line of sight abundances using a technique outlined in Irvine et al. (1987). H_2 does not emit appreciably at the cold temperatures associated with these objects ($T \sim 10$ K). Therefore optically thin isotopologues of CO, generally C^{18}O , were used as surrogates to trace the H_2 column density with previously calibrated abundances (e.g. $x(\text{C}^{18}\text{O}) \sim 1.7 \times 10^{-7} \equiv n(\text{C}^{18}\text{O})/n(\text{H}_2)$; Frerking et al. 1982). These studies strongly aided the interpretation that chemical reactions between ions and molecules dominate the gas-phase chemistry (Herbst 2005).

In parallel to gas-phase chemical studies, the fundamental vibrational modes of solid state molecules such as H_2O and CO were detected in the ISM (Gillett & Forrest

1973; Lacy et al. 1984). Many studies of molecular ices frozen on the surfaces of dust grains have been conducted towards embedded sources which provide a strong infrared background to study foreground ices (e.g. van Dishoeck 2004). To provide important insight on ices in cold gas, observations of bright field stars located behind molecular cloud material (with extinctions ≤ 20 mag) are used as candles that probe material remote from embedded sources (Whittet et al. 1988). Icy mantles coating grains in ambient gas are dominated by H₂O ice with substantial amounts of CO and CO₂ at a level of $\sim 25\%$ of the water ice abundance in each case (Gibb et al. 2004).

There exists a threshold extinction below which the ice features are not seen, implying that grains are not mantled at low extinction. This threshold varies for each ice component and is different between various clouds. In Taurus, the water ice threshold is $A_V^{th}(\text{H}_2\text{O}) = 3.2^m \pm 0.1^m$; a comparable threshold is observed for CO₂ ice but for CO $A_V^{th}(\text{CO}) = 6.8^m \pm 1.6^m$ (Whittet et al. 2001; Bergin et al. 2005; Whittet et al. 2007). The threshold value presumably is related to the formation mechanisms for ices and in Taurus the relatively low water ice threshold may imply that the water ice forms at a low density where atomic H is available. These observations further demonstrate that ices constitute a substantial fraction of the available carbon and oxygen (van Dishoeck and Blake 1998). Thus CO (and its isotopologues) is not a reliable tracer of the H₂ column when using previously calibrated abundances. In addition, it is clear that grains can act as a catalyst for chemistry on the surface, producing both simple and complex molecules as part of an interchange between the gas and solid phases (Tielens & Hagen 1982; Herbst et al. 2005).

4.2 Observational Chemistry

4.2.1 GAS-PHASE FREEZE-OUT As discussed in §3 a sample of low-mass starless cores are now known with well described physical structure as a function of position: $N_{\text{H}_2}(r)$, $n_{\text{H}_2}(r)$, $T_{\text{dust}}(r)$, $T_{\text{gas}}(r)$. Sample profiles are given in Fig. 4. Foremost among these are the two new template objects: L1544 and B68. There are some caveats to the determination of each of these parameters, but the overall structure is well characterized and has led to significant advances in our understanding of the chemistry. In general there are two factors that influence these gains. (1) Using the dust mm/submm continuum emission as a surrogate for the H₂ distribution allows for an examination of molecular abundance variations directly relative to H₂. This is a fact noted by Mezger et al. (1992) in the high-mass NGC2024 star forming region. However, the presence of embedded sources can substantially influence the dust emission morphology, potentially leading to different conclusions (Chandler & Carlstrom 1996). While starless cores do have small thermal gradients (§3.2) this particular complication is minimized. (2) Molecular emission depends on the H₂ density, gas temperature, and on the abundance. Using sophisticated one-dimensional radiation transfer codes (Monte-Carlo or Accelerated Lambda Iteration; Bernes 1979; Rybicki & Hummer 1991) and the density and temperature *structure* as inputs, the abundance profile along the line of sight can be constrained for the first time.

Initial studies found the first direct link between chemistry in the gas and interactions with grain surfaces by simply comparing the estimated CO and CCS column densities to the H₂ column estimated from the dust (Kuiper et al. 1996; Willacy et al. 1998; Kramer et al. 1999; Caselli et al. 1999). This is interpreted

as evidence from gas-phase data that the CO molecules are freezing onto grain surfaces. A comparative study of CO suggest freeze-out dominates when densities exceed $\sim 3 \times 10^4 \text{ cm}^{-3}$ (Bacmann et al. 2002).

Spatial mapping of ices within individual cores supports the interpretation of the gas-phase observations as the abundance of CO ice is found to significantly increase when densities exceed $\sim 10^5 \text{ cm}^{-3}$ (Pontoppidan 2006). Near the core center the abundance is close to the typical gaseous CO abundance of 10^{-4} , indicating that the majority of CO is frozen out. Furthermore, the abundance of water ice is typically $0.5 - 0.9 \times 10^{-4}$ except at the highest densities where the abundance increases (Pontoppidan et al. 2005). The molecular ices are therefore substantial reservoirs of the available oxygen.

4.2.2 SELECTIVE FREEZE-OUT Molecular surveys reveal further differences, Fig. 7 shows a sample of this work with a comparison of the $850\mu\text{m}$ dust continuum distribution in the Barnard 68 starless core with molecular emission traced by C^{18}O and N_2H^+ . In this core the N_2H^+ emission more closely follows that of the dust than does C^{18}O , which appears as a “semi-ring-like” structure around the dust and N_2H^+ emission maximum (Bergin et al. 2002). Tafalla et al. (2002) surveyed 5 cores in Taurus (including L1544) illustrating general characteristics of core chemistry: carbon-bearing species, represented by CO and CS deplete from the gas while nitrogen-hydrogen bearing molecules, N_2H^+ and NH_3 trace the core center (see also Caselli et al. 1999). From the abundance profile it is estimated that the CO and CS abundance traces a large dynamical range with declines of at least 1-2 orders of magnitude in the core centers relative to the lower density core edge, while the abundances of nitrogen molecules either stay constant or decay more slowly. The interpretation of “selective” freeze-out, where molecules exhibit different behavior in terms the response of the chemistry to interactions with grain surfaces, naturally explains some long-standing issues such as the emission differences seen between carbon and nitrogen molecules described earlier (compare Swade 1989; Pagani et al. 2005), and the larger core sizes and velocity dispersions seen for CO and CS when compared to earlier NH_3 data (Zhou et al. 1989; Tafalla et al. 2002). For star formation this isolates the nitrogen hydrides as the key probes of dense gas.

4.2.3 CARBON, OXYGEN, AND NITROGEN Cores with well defined physical properties have clarified additional outstanding chemical issues regarding carbon, oxygen, and nitrogen chemistry. It is clear that CO represents the major reservoir of carbon in the gas and, along with CO_2 , in the grain mantle. Maret et al. (2006) demonstrated that N_2 is not the dominant carrier of nitrogen in molecular gas. They suggest that N I as a main reservoir of atomic nitrogen (see also van Dishoeck and Blake 1998); however, at present, it is unclear what is the predominant form of gas-phase nitrogen. Observations by the *Submillimeter Wave Astronomy Satellite* (SWAS) and *Odin* also demonstrated that the abundance of ortho-water vapor and molecular oxygen is well below theoretical expectations throughout the Galaxy (Snell et al. 2000; Hjalmarson et al. 2005) and in starless cores in particular (Bergin & Snell 2002). Due to atmospheric absorption, para-water vapor has yet to be observed and the limits on the water abundance disagree with pure gas-phase chemical theory provided that the ortho/para ratio is not below the equilibrium value at 10 K ($\text{o-H}_2\text{O}/\text{p-H}_2\text{O} \sim 0.3$). The low water vapor abundance is interpreted as the result of water ice formation on grain surfaces. At grain temperatures below $\sim 110 \text{ K}$ (§4.3.2) water will remain frozen on

grains, which indirectly lowers the gas phase atomic oxygen abundance thereby hindering formation of water and molecular oxygen in the gas (Bergin et al. 2000; Charnley et al. 2001). Further analysis suggests that the water vapor emission likely arises from the surface photodissociation region where a balance between photodesorption of water ice and photodissociation of water vapor exists (OH should behave in a similar fashion) (Melnick & Bergin 2005). The launch of the Herschel Space Observatory, which will be capable of observing both ortho- and para-water will provide definitive information on the water abundance and its potentially defining role in gas-phase freeze-out.

4.3 Chemical Theory

4.3.1 BASIC PROCESSES In the literature the loss of gaseous molecules to the solid phase is often labeled as depletion, which implies a lowering of the gas-phase abundance, or as freeze-out, which is more direct statement of the process. In practice both terms can be used, but there are some nuances. While neutral species freeze onto grain surfaces it is not thought that molecular ions behave in a similar fashion. Grains in dense clouds are believed to carry negative charge (Weingartner & Draine 2001). The ion-negatively charged grain recombination releases a few eV which, if carried by the products, significantly exceeds the molecule-grain binding energies of $\sim 0.1 - 0.5$ eV (Collings & McCoustra 2005). Thus ions can deplete, via, for example, gas phase processes and by pre-cursor molecules (e.g. CO for HCO^+) adsorbing onto grains, but do not freeze-out.

Atoms and molecules freeze onto grain surfaces or adsorb with a rate of $k_{fo} = \sigma v n_g S \text{ s}^{-1}$. Here σ is the grain cross-section (generally assuming to be an average grain with a $0.1 \mu\text{m}$ radius), v is the mean velocity of the Maxwellian distribution of gaseous particles, n_g the space density of grains, and S is the sticking coefficient (i.e. how often a species will remain on the grain upon impact). Using relevant parameters for CO at 10 K (assuming $S = 1$ as suggested by laboratory experiments; e.g. Bisschop et al. 2006) the freeze-out timescale $\tau_{fo} = k_{fo}^{-1} \sim 5 \times 10^9 / n_{H_2} (\text{cm}^{-3}) \text{ yrs}$. Once on the grain, molecules can react with any species that is mobile on the grain surface at 10 K, such as atomic hydrogen, or if a species is saturated (e.g. H_2O , NH_3 , CO_2) it will remain inert on the surface. For cold dense gas that is shielded from external radiation the physical processes that can remove or desorb molecules from grain surface are either inactive or can only desorb the most volatile ices (see van Dishoeck and Blake 1998, for a complete summary of desorption processes). In cold cores it is thought that energetic cosmic ray impacts can desorb the most volatile ices (e.g. CO but not H_2O ; Leger et al. 1985; Hasegawa and Herbst 1993; Bringa & Johnson 2004). Thus the dominant effect is the adsorption of atoms and molecules onto grain surfaces and any subsequent consequences that result from this interaction.

4.3.2 CHEMICAL AND DYNAMICAL TIMESCALES In Fig. 8 we compare relevant chemical and dynamical timescales. Representative dynamical timescales are provided for free-fall and ambipolar diffusion, the latter having been suggested as a primary mode of core condensation (Shu, Adams & Lizano 1987). The free-fall timescale is $\tau_{ff} = [3\pi/32G\rho]^{0.5} \sim 4 \times 10^7 / n_{H_2}^{0.5} \text{ yrs}$ and the ambipolar diffusion timescale is discussed in § 4.4.2. The gas-phase chemical timescale is set by cosmic rays and has a constant dependence on the density, while freeze-out has linear dependence on the density. The evaporation rate is given by the Polanyi-Wigner relation (Tielens 2005):

$$\tau_{\text{evap}} = \nu_0^{-1} \exp(E_b/kT) \text{ (s}^{-1}\text{)} \quad (1)$$

where ν_0 is the vibrational frequency of the molecule in the potential well (typically $\sim 10^{12} \text{ s}^{-1}$) and E_b is the binding energy. The evaporation timescale has an exponential dependence on the dust temperature, but critically depends on the binding strength to the grain surface or mantle. Measured binding energies for CO-CO are $\sim 820 \text{ K}$ (Collings et al. 2003) and $\sim 5800 \text{ K}$ for H₂O-H₂O (Fraser et al. 2001), implying evaporation temperatures of $\sim 15 \text{ K}$ for CO and $\sim 110 \text{ K}$ for H₂O at $n_{\text{H}_2} = 10^5 \text{ cm}^{-3}$ and assuming a typical $0.1 \mu\text{m}$ grain abundance of $x_{\text{gr}} = 10^{-12}$. Fig. 8 demonstrates a key aspect of starless cores - as cold objects, $T_{\text{dust}} \sim T_{\text{gas}} \sim 10 \text{ K}$, evaporation is unimportant, with timescales $> 10^8$ yrs. Furthermore the freeze-out timescale becomes shorter than the free-fall and ambipolar diffusion timescales as the density increases. Thus as the core physically evolves, the effects of freeze-out on gaseous species are magnified, and can be used to constrain the mechanism of core formation.

4.3.3 CHEMICAL/DYNAMICAL MODELS Combined chemical and dynamical models follow the chemical composition as the core contracts. Such models generally adopt parameterized fits or a more direct coupling to simple dynamical models (e.g. Larson 1969; Penston 1969; Shu 1977; Basu & Mouschovias 1994). Notable chemical/dynamical models are Rawlings et al. (1992), Bergin & Langer (1997), Aikawa et al. (2001) and Li et al. (2002). With basic gas-grain microphysics incorporated into time-dependent models (see Tielens 2005) the chemical structure discussed in § 4.2.2 can be explained and, in some cases, was predicted.

Basic elements of the chemistry are illustrated in Fig. 9. During collapse or condensation, the central regions of the core increase in density to levels where neutrals rapidly freeze onto grains ($n_{\text{H}_2} > 10^5 \text{ cm}^{-3}$). This contrasts with the lower density less evolved core edges with undepleted abundances. As collapse proceeds these effects become amplified (compare the two times provided for CO in Fig. 9). Bergin & Langer (1997) first showed that carbon- and sulphur-bearing species (e.g. CO, CS, CCS) suffer the greatest effect from depletion. In contrast the nitrogen hydride pool is the least affected (see also Aikawa et al. 2001). At first this was assumed to be due to a lower binding strength of N₂ (the precursor molecule for both N₂H⁺ and NH₃) to the grain surface than for CO. This has now been measured to be equivalent to CO (Öberg et al. 2005).

It is now recognized that the observational appearance of selective freeze-out can be separated into first-order chemical effects, the direct freeze-out of neutrals (e.g. CO, CCS, CS, N₂), and second-order effects, changes created by the imbalance in the chemistry left primarily by the loss of gaseous carbon monoxide. CO is a major destroyer of molecular ions and its removal from the gas leads to a change in the relative abundance of major charge carriers (Rawlings et al. 1992). Particularly affected is the H₃⁺ ion, the precursor to molecular ions such as N₂H⁺ and HCO⁺ that are the respective daughter products of N₂ and CO. These key observable ions (N₂H⁺ and HCO⁺) will also decrease in abundance as the parent molecules freeze-out; however, CO is a major destroyer of N₂H⁺ and as CO disappears from the gas there is a subsequent increase in abundance of N₂H⁺ (Aikawa et al. 2001; Bergin et al. 2002; Jørgensen et al. 2004). NH₃ then forms from N₂H⁺ (Geppert et al. 2004; Aikawa et al. 2005). Thus the abundance of the nitrogen hydrides is strongly enhanced and these species are probing the gas where CO (and other carbon-bearing species) are depleting. An important

point here is that the abundance of both NH_3 and N_2H^+ are several orders of magnitude below the abundance of molecular nitrogen. N_2 is freezing onto grains at the same level as CO. Provided the N_2 abundance does not deplete to levels below N_2H^+ and ammonia, then these tracers can still form and emit from layers where commonly observed tracers of dense regions have significantly reduced abundances.

Combined models reproduce not only the pattern of depletions, but also the column densities observed in L1544 (Aikawa et al. 2001; Li et al. 2002). In general models obtain best agreement with collapse timescales much shorter than would proceed from ambipolar diffusion starting from a magnetically subcritical state (e.g. Walmsley et al. 2004); however there is some disagreement (Li et al. 2002). A clear point is that evolutionary timescales at densities near $\sim 10^4 \text{ cm}^{-3}$ cannot be much longer than $\sim 0.5 - 1 \text{ Myr}$ as significant CO freeze-out would be produced at densities below where it is observed (Flower et al. 2005; Tafalla et al. 2006). Moreover, collapse cannot be too fast ($> 0.2 \text{ km s}^{-1}$ at $\tau_{\text{dyn}} \lesssim 5 \times 10^5 \text{ yrs}$)¹ or there will be less depletion and emission linewidths would be too broad (Myers 1983).

Current work has greatly benefited from laboratory work on low temperature gas phase reactions, grain binding energies, and on surface catalysis (Florescu-Mitchell & Mitchell 2006; Collings & McCoustra 2005; Nagaoka et al. 2005; Bisschop et al. 2006; Hornekaer et al. 2003; Katz et al. 1999). Moreover the recent re-calculation and extension of collisional rates of astrophysically important molecules is of great use and deserves mention (Dubernet & Grosjean 2002; Flower 2001; Daniel et al. 2005). However, large questions remain regarding the nature of the grain surface catalysis in this cold environment and the strength of the mechanisms that could return molecules to the gas (e.g. Leger et al. 1985; Bringa & Johnson 2004; Shen et al. 2004). It is also unclear how complex molecules form in the gas-phase. For example CH_3OH is detected in cold clouds, but currently has no known gas-phase formation route. An examination of the extent of the complex chemistry in cores with well defined properties is needed and will likely lead to gains in our understanding of interstellar organic chemistry (see Hirota et al. 2004).

One clear positive statement is our knowledge of the chemistry and the time sensitive nature of the gas-grain interaction is such that we now have the methods to place relative ages between cores within a given sample (Hirota et al. 2002; Tafalla & Santiago 2004). This should aid in our analysis of the core/star formation process. Moreover, the combination of chemical/dynamical models with radiative transfer (see Lee et al. 2004, as an example) offers the best opportunity to take these models to the next level and truly begin to test star formation theory.

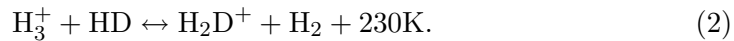
4.4 Deuterium Chemistry and the Ionization Fraction

4.4.1 DEUTERIUM FRACTIONATION Another second-order effect induced by the CO freeze-out is a sharp rise in the level of deuterium fractionation. Enhancements of deuterium bearing molecules relative to the hydrogen counterparts has been known for some time (Guelin et al. 1982). In cold clouds enrichments of

¹The typical non-thermal linewidth in starless cores (e.g. L1498, L1517B, B68, ...) is 0.2 km/s . If this represents a purely inward motion, it would correspond to an infall speed of 0.1 km/s at most. With a typical core radius is 0.05 pc , this implies a typical contraction time of 0.5 Myr .

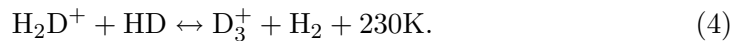
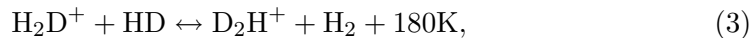
2-3 orders of magnitude are observed above the atomic hydrogen value of $(D/H) \geq (2.3 \pm 0.2) \times 10^{-5}$ estimated within 1 kpc of the Sun (Linsky et al. 2006). Because of the lower zero point energy of deuterium bonds compared to bonds with hydrogen, ion-molecule reactions in the dense ISM are thought to be the mechanism responsible for these enrichments (Millar et al. 1989). Deuterium enrichments can also be created via reactions on the surfaces of dust grains (Tielens 1983; Nagaoka et al. 2005), but in these cold cores freeze-out is believed to dominate as opposed to sublimation (e.g. freeze-out dominates the chemistry of the volatile CO molecule).

In the cold dense ISM, deuterium chemistry is driven by the following reaction:



The forward reaction is slightly exothermic favoring the production of H_2D^+ at 10 K, enriching the $[D]/[H]$ ratio in the species that lie at the heart of interstellar ion-molecule chemistry (Millar et al. 1989)². These enrichments are then passed down the reaction chains to species such as DCO^+ , DCN , $HDCO$, and others.

Pure gas-phase models without freeze-out cannot produce significant quantities of doubly (NHD_2 ; Roueff et al. 2000) and triply deuterated ammonia (ND_3 ; Lis et al. 2002) as observed in starless cores. This motivated a re-examination of the basic deuterium chemistry. The primary advance in our understanding is two-fold: (1) deuteration reactions do not stop with H_2D^+ , rather they continue towards the formation of both D_2H^+ and D_3^+ , via a similar reaction sequence (Phillips & Vastel 2003; Roberts et al. 2003; Walmsley et al. 2004):



(2) The freeze-out of CO, which is primary destroyer of both H_3^+ and H_2D^+ , increases the rate of the gas phase fractionation reactions (see deuterium species in Fig. 9; Stark et al. 1999; Aikawa et al. 2001; Bacmann et al. 2003). This inference is strongly supported by the detection of H_2D^+ and D_2H^+ in starless cores (Caselli et al. 2003; Vastel et al. 2004; van der Tak et al. 2005), as illustrated in Fig. 10.

The creation of multiply deuterated ions leads to the production of high deuteration levels similar to those observed. An additional by-product is an enhanced atomic (D/H) ratio which will accrete onto grains and be available for surface reactions (Tielens 1983; Charnley et al. 1997; Stantcheva and Herbst 2003; Aikawa et al. 2005) creating molecules rich in deuterium to be exposed when ices sublimate off warm grains as the result of stellar birth. However, the extent of the surface deuteration opposed to the gas phase needs to be further explored. It is worth emphasizing that the observed form of H_2D^+ in interstellar clouds is ortho- H_2D^+ and models show that the H_2D^+ ortho/para ratio (o/p) will change with density and is a sensitive function of the molecular hydrogen ortho/para ratio (Flower et al. 2006). If the H_2 o/p ratio is not in equilibrium at the low $T_g < 20$ K (where $o/p \ll 1$) and instead is near 3:1, then deuterium fractionation will not work (Pineau des Forets et al. 1991; Gerlich et al. 2002). Observations

²Reaction 2 has been measured in the lab at low temperatures finding that there is an additional dependence on the ortho/para ratio of H_2 (Gerlich et al. 2002).

from the Spitzer Space Telescope suggest that the H_2 o/p ratio is in equilibrium in cold pre-shock gas (Neufeld et al. 2006), a fact consistent with the observed fractionation. Herschel and SOFIA will be needed to constrain the H_2 o/p ratio via observations of ortho- and para- H_2D^+ in starless cores.

4.4.2 IONIZATION FRACTION For subcritical starless cores (where the magnetic field supports the cloud against gravity, 2.7) the evolutionary timescale is set by ambipolar diffusion and the ion fraction is a critical factor in determining the magnetic flux leakage. McKee (1989) discussed the various charge carriers and recombination rates deriving a basic expression that has wide use: $x_e = 1.3 \times 10^{-5} n(\text{H}_2)^{-0.5}$. The effects of freeze-out can alter both the pre-factor and the exponent of the density dependence (Bergin & Langer 1997; Caselli et al. 2002c; Walmsley et al. 2004), but see also Ciolek & Mouschovias (1998).

Past studies of the ion fraction in dense cores focused on the $\text{DCO}^+/\text{HCO}^+$ ratio, that was predicted to be a sensitive function of the electron abundance. Furthermore, it was thought that HCO^+ was a major charge carrier throughout the core (e.g. Caselli et al. 1998; Williams et al. 1998). These studies found line of sight average ion fractions of $x_e \sim 10^{-7}$ (relative to H_2), implying weak coupling to the magnetic field. One variable assumption in models is the presence or absence of metal ions (e.g. Fe^+ , Mg^+ , ...), which have slower recombination timescales than molecular ions. If present, metals could dominate the electron fraction over molecular ions ultimately produced by cosmic ray impacts. Currently detailed models imply no significant contribution from heavy metal ions to the electron fraction (Caselli et al. 2002c; Maret et al. 2006).

Due to the freeze-out of neutrals, HCO^+ does not trace the core center and major charge carriers in the core center are likely to be a combination of H_3^+ , H_2D^+ , D_2H^+ , and D_3^+ . An example of the “typical” ionization structure is given in Fig. 11. When illuminated by the standard interstellar radiation field or below, the ionization is high at core edges ($A_V < 1\text{--}2$ mag) due to CO photodissociation and ionization of carbon. Deeper in the cloud the regime of cosmic ray ionization leads to an ion fraction that decays with increasing density. For the densest ($n_{\text{H}_2} > 10^6 \text{ cm}^{-3}$) most evolved cores the ultimate expectation is that D_3^+ is the dominant ion (Roberts et al. 2003; Walmsley et al. 2004). Observations and models now suggest that in at least some objects the ion fraction in the core center is quite low, $x_e \sim 3 \times 10^{-9}$, implying that the gas is locally decoupled from the field (i.e. the timescale for ambipolar diffusion is comparable to or less than the free-fall time, Caselli et al. 2002c; van der Tak et al. 2005).

Walmsley et al. (2004) and Flower et al. (2005) discussed ambipolar diffusion timescales in the context of depletion, providing detailed expressions:

$$\tau_{ad} \sim \frac{2}{\pi G m_{\text{H}_2}^2} \sum_i \frac{n_i}{n_{\text{H}_2}} \mu_{in} < \sigma v >_{in} \text{ yr} \quad (5)$$

where G is the gravitational constant, i implies a summation of ionic species, $\mu_{in} = m_i m_{\text{H}_2} / (m_i + m_{\text{H}_2})$ is the reduced mass with H_2 the neutral collision partner. The rate coefficient for momentum transfer between ions and neutrals is assumed to be $< \sigma v >_{in} = \pi e (\alpha / \mu_{in})^{0.5}$, with α as the polarizability of H_2 (Osterbrock 1961). If HCO^+ is the dominant ion then $\tau_{ad} \sim 1.7 \times 10^{14} x_e$. An essential feature is that the timescale is proportional to the square root of the reduced mass implying that the ionic composition also influences the diffusion of magnetic flux (the timescale is $\sim 60\%$ lower if H_3^+ dominates and 25% for D_3^+).

These works highlighted the potential of negatively charged grains to alter the degree of ionization and also as limiting factors in deuterium fractionation, which can be influenced by the changing size distribution as the result of coagulation.

4.5 Key Tracers and the Possibility of Complete Heavy Element Depletion

Starless cores have revealed a dynamic and evolving chemical structure that highlights key tracers that probe different depths and evolutionary times. One open possibility is that all heavy elements are depleted in core centers prior to stellar birth. This has important implications for our ability to study the process because the heavy element species (e.g. CO, CS, N_2H^+ , ...) have permanent dipole moments and can be observed via pure rotational transitions in regions of the atmosphere with good transmission via heterodyne techniques at mm wavelengths. If the timescales of star formation are such that heavy element depletion occurs prior to the formation of a point source then our ability to study the entire process will be severely hampered, leaving only hydrogen/deuterium molecules with dipole moments as probes (H_2D^+ , D_2H^+).

At present the evidence for total heavy element depletion is inconclusive and focused on the question of whether N_2H^+ is seen to deplete. This molecule is key as it also is the likely formation route of NH_3 , and if it depletes then ammonia should follow suit. Bergin et al. (2002) and Maret et al. (2006) find that N_2H^+ does drop in abundance towards the center of the B68 core. In contrast, the N_2H^+ and NH_3 emission in L1544 when observed in high resolution appears to coincide with the continuum emission peak (Williams et al. 1999, Crapsi et al. 2006, in prep.). Thus in the two best studied sources we find contradictory solutions and total heavy elemental depletion remains an intriguing possibility.

Given the gains in our understanding of the chemistry and how it changes with core evolution, in Fig. 12 we provide a schematic to summarize our current knowledge. For less evolved sources ($n_{r=0} < \text{few} \times 10^4 \text{ cm}^{-3}$) the effects of depletion are likely minimized and commonly observed molecules such as CO, C^{18}O , CS, and HCO^+ , remain viable tracers. For evolved sources ($n_{r=0} > \text{few} \times 10^4 \text{ cm}^{-3}$) species such as N_2H^+ , NH_3 , N_2D^+ , and DCO^+ appear to be the best molecular probes of core gas, perhaps even to the dense center. Regardless of whether total heavy element depletion has occurred, both H_2D^+ and D_2H^+ are unambiguous tracers of the densest gas. In contrast, emission from C^{18}O , CS, H_2O , and HCO^+ preferentially sample the core edge.

5 INFRARED DARK CLOUDS

5.1 Background

Infrared dark clouds (IRDC) were discovered serendipitously in mid-infrared surveys of the galactic plane by the Infrared Space Observatory's ISOGAL survey (Perault et al. 1996)³ and the Midcourse Space Experiment (MSX; Egan et al. 1998)⁴. Both surveys revealed a population of objects that were dark at mid-infrared wavelengths with opacities ranging from 1–4 at 8 and 15 μm (Carey et al.

³ISOGAL consisted of a 7 and 15 μm survey of 12 degrees in the plane interior to $|l| = 45^\circ$.

⁴MSX surveyed from $l = 91 - 269^\circ$ with $b \pm 5^\circ$ in 5 filters sampling between 4 – 25 μm . IR dark clouds are best seen in MSX Band A images.

1998; Hennebelle et al. 2001). The objects appear to be quite filamentary and comparison with IRAS suggests that the objects were dark from $7 - 100 \mu m$ and “represent a population of heretofore unrecognized population of cold, dense, isolated clouds” (Egan et al. 1998; Hennebelle et al. 2001). A compilation of MSX dark objects finds over 10,000 sources with kinematic distances between 1–8 pc with a distribution that peaks towards prominent star forming regions, spiral arm tangents, and the 5 kpc Galactic Molecular Ring (Simon et al. 2006). Fig. 13 presents one example showing the G11.11-0.12 IRDC as seen by the Spitzer Space Telescope and in sub-millimeter continuum emission.

Much of the interest generated by this discovery has focused on the formation of high-mass stars and stellar clusters. This review demonstrates many of the gains in our knowledge of the formation of low-mass stars through the isolation of starless cores as a unique sample to study the initial conditions of star formation. In the case of clustered star formation the nearest region is Orion at ~ 500 pc and it is unclear how representative Orion is when compared to star formation in the inner galaxy, where most of the molecular mass resides. IRDC’s provide the capability to examine the early stages of star cluster formation beyond the local solar neighborhood. The primary issue for massive star formation is that the timescales are much faster when opposed to the formation of solar mass stars. Thus there will be fewer pre-stellar massive objects present at any given time to isolate. Moreover, since massive stars are born in more distant clouds with stellar clusters the chances of confusion are greater (for a nice review, see Garay & Lizano 1999). The discovery of infrared dark clouds provides a new – greatly expanded – sample to search for the precursors to massive stars. Without constraining observations, theories of massive star formation are divided between models that suggest that high mass stars form by accretion of an extended envelope or competitive accretion of cluster stars for remaining unbound gas, with stars located near the central potential obtaining higher masses (Krumholz et al. 2005; Bonnell & Bate 2006). A discussion of the theoretical issues is beyond the scope of this review and the reader is referred to the cited references and the contribution by Yorke & Zinnecker in this volume.

5.2 Physical Properties and Implications

The properties of infrared dark clouds have been estimated using a variety of techniques that have been outlined in §3 and Evans (1999). From observations of CO, NH₃, CH₃C₂H, and H₂CO temperatures are estimated to be below 20 K with densities in excess of 10^5 cm^{-3} (Carey et al. 1998; Teyssier et al. 2002; Pillai et al. 2006). Surveys of mm/submm continuum emission and N₂H⁺ constrain typical core masses of 100-1000 M_⊙ and sizes of $R \sim 0.3 - 0.7$ pc which are comparable to those of molecular cores containing embedded high-mass protostellar objects. (Sridharan et al. 2005; Ragan et al. 2006; Rathborne et al. 2006). The cores are dominated by turbulence with velocity linewidths of $\sim 2 - 3 \text{ km s}^{-1}$. These linewidths are systematically less than seen towards cores with embedded protostars, which is similar to the dependence observed in local clouds (Sridharan et al. 2005; Ragan et al. 2006). The core mass spectrum has a power-law slope of 2.1 ± 0.4 (Rathborne et al. 2006), which is comparable to the Salpeter IMF; however, it is likely that these objects will fragment on scales below the observed resolution ($11''$), and this value is also consistent with the CO mass spectrum of molecular clouds (§2.3.4). Based on current evidence, it is clear

that these sources likely represent the birth sites of stellar clusters and that a sub-sample must be forming massive stars.

The implications of IRDC's for galactic star formation have been discussed by Rathborne et al. (2006) who estimate that the star formation rate in these objects is $\sim 2 M_{\odot}/\text{yr}$. This is comparable to the total Galactic rate of 3–5 M_{\odot}/yr (Prantzos & Aubert 1995) and hints that this population is responsible for current star formation in the Milky Way. The full promise of these objects will be realized as Spitzer galactic plane surveys (GLIMPSE and MIPS GAL) are analyzed and sensitive high resolution instruments are brought to bear (e.g. CARMA, PdB, eVLA, ALMA) to provide the kind of spatial resolution that is currently available towards the Orion Molecular Cloud. Such observations, when combined with the techniques developed for local starless clouds described in §3–4, will ultimately aid in constraining the fragmentation of molecular clouds and the eventual formation of stellar clusters including massive stars.

6 SUMMARY AND FUTURE PROSPECTUS

Cold Dark Clouds are a fundamental component of the galactic interstellar medium. They represent the nearest sample of star-forming molecular material, and as such, they play a key role in unraveling the still mysterious process via which stars and planetary systems are born. As this review has shown, the study of dark clouds has seen some significant progress but still contains significant areas of uncertainty.

On the large parsec-scale, high resolution maps of optical and infrared extinction have provided a needed “big picture” look at cloud structure, and have determined that a significant amount of material lies at low extinction ($A_V < 3-5$). Complementing these data are maps of molecular emission where, aided by improved sensitivity and mm-wave heterodyne arrays, we can probe deeper using ^{13}CO and C^{18}O than allowed by optically thick ^{12}CO lines. These data have highlighted the filamentary and irregular structure of molecular clouds, suggestive of a transient nature. The velocity structure, on the other hand, tells a tale of the dominance of turbulence, and sophisticated techniques to characterize gas motions have constrained the spectrum of turbulence allowing us to move one step beyond Larson’s Laws. Magneto-hydrodynamic models have matured to the point where they can produce realistic turbulence, and numerous simulations have shown that the decay of MHD turbulence is rapid and unavoidable without a continuous source of replenishment. This raises an important challenge to established theories of long-lived clouds (> 10 Myr). In addition to turbulence, static magnetic fields are a potentially important ingredient of cloud physics. Measurements of this field show that in some instances the polarization vectors follow cloud structure, but the measurement and interpretation are complicated by various effects.

In regions where turbulence has dissipated, dense self-gravitating cores form. By mapping their molecular line and dust continuum emission, we have found that cores are characterized by a central region with near constant density and gas temperature (to within a factor of 2), together with subsonic motions. Bonnor-Ebert spheres often provide accurate fits to the observed emission, and although they represent a simplification of the core physics, they should be considered the best available starting point for numerical models of core evolution. As in the

case of the large-scale, the role played by the magnetic field is still uncertain. In addition, detailed radiation transfer analysis suggest the presence of motions along the line of sight. These motions may have an inward component that is associated with core condensation, but often contain additional contributions of an unknown origin. Core-envelope velocity differences, pulsation, or rotation may be responsible for them.

Knowledge of core physical structure has revealed the complex chemical composition of starless cores. Observations demonstrate that chemical inhomogeneities are an inherent dense cold core characteristic that needs to be considered when interpreting molecular line data. The combination of sophisticated radiation transfer codes and realistic core physical structures allows, for the first time, the investigation of line of sight chemical gradients. As a result, it has been found that gas-grain interactions dominate the chemistry of cores, and this has a number of consequences. The primary effect is the freeze-out onto grains of important gaseous species, such as CO. This removal of CO from the gas phase leads to the production of new species, like N_2H^+ and NH_3 , in the denser gas where these effects are dominant. In addition, the deuterium fractionation of the core is greatly enhanced, as multiply-deuterated molecules are produced via reactions that begin with H_2D^+ , D_2H^+ , and D_3^+ . Thanks to this new understanding of the core chemistry, the observed abundance profiles are beginning to be successfully reproduced by models that combine chemistry and dynamics of core contraction. Using these models we can now isolate molecular probes that target specific regions along the line of sight. For example, two classical probes of core structure, CO and CS, are now understood to be only tracers of the low density cloud surface. Deeper layers of the core are traced by N_2H^+ and NH_3 (along with their deuterated daughter products), while the center is unambiguously traced by H_2D^+ and D_2H^+ . These chemical signatures change as a function of core evolution and may help to trace the history of gas contraction.

Within this review we have highlighted areas where progress is needed, and here we discuss some areas where breakthroughs could occur using future instruments and advance techniques. For the most part we are concentrating on issues that can be addressed via observations.

- There is considerable need to connect the molecular cloud component with the atomic diffuse interstellar medium. This may illuminate the question of cloud formation, cloud destruction, and the origin of the turbulence in molecular clouds, and it will require the combination of mapping observations of H I, extinction, [C II], and CO emission.
- To address the issue of cloud fragmentation and the potential breakdown in hierarchical structure, it is required that clouds are mapped with a uniform tracer from the large to the small scales. The most likely tracer for this work would be the dust continuum emission, if observations retain sensitivity to large scale structure, and SCUBA-2 offers the best opportunity in this regard. Molecular tracers will provide needed velocity information. Unfortunately, a wide variety of disparate techniques is currently used to analyze the rich information contained in 3-D data cubes. A common description of cloud structure is clearly needed both to inter-compare observations of different clouds and to test numerical simulations.
- The transition from turbulent cloud to the quiescent core regime is a critical element in the evolution towards star formation. In this transition,

turbulence dissipates and the cores acquire the flattened density profiles reminiscent of Bonnor-Ebert spheres. Whether the observed subsonic motions represent a key part of this transition should be explored. For this, an improved understanding of the chemistry should help in the selection of a number of molecular tracers to probe different layers. To track turbulent dissipation, a number of cores spanning a range of evolutionary states needs to be isolated and characterized. Millimeter observations with existing and future radio telescopes, preferably with large format heterodyne receiver arrays (e.g. SEQUOIA on LMT), offer the potential to examine these issues.

- A clear advance results from the ability to combine measurements of the dust column spanning a range of wavelengths from near-IR absorption to submm emission to examine the dust properties, in particular the mass opacity coefficient. In parallel to understanding how the gas changes with contraction there is an open question as to how dust properties change as the mantles grow and grains coagulate. Herschel and SOFIA observations should aid to disentangle the coupled effects of dust temperature and emissivity on dust emission/absorption.
- Models and observations have mapped a chemical sequence that can track the relative evolutionary status of condensing cores. Observations can be used to provide a rough indication of the evolutionary state, but improved theoretical models are still needed to provide core studies with an accurate chemical clock to test core condensation theories. Further testing of models against observables (e.g. integrated emission and line width) also requires accurate collisional rates, molecular rest frequencies, measurements of low temperature gas phase reaction rates, and studies of the gas-grain interaction in the laboratory.
- It is not clear yet whether the centers of cores are completely depleted in key elements (C, O, and N) preceding the onset of gravitational collapse, and this has important implications in the ongoing search for star-forming infall. Herschel, SOFIA, and especially ALMA will be important instruments to clarify this issue.
- The emerging field of infrared dark clouds holds the promise of unlocking the secrets of massive star formation, which is an area with considerable theoretical controversy. At present it is not certain how IRDC's fit into our picture of Giant Molecular Clouds. Are these sources the dense centers of clouds in the Galactic molecular ring, and if so, how do they compare in properties (mass spectrum, size, clumping/fragmentation, turbulence) to the local population of massive star-forming regions exemplified by Orion? Systematic studies with high resolution ($< 4''$) are needed to bring the study of these objects to the level of detail that currently exists for local clouds. eVLA and ALMA will be important in this regard.

ACKNOWLEDGMENTS

We thank Y Aikawa, P Caselli, M Heyer, P Myers, M Walmsley, and J Williams for reading portions of the manuscript and providing useful comments. E van Dishoeck gave the manuscript a thorough reading and suggested a number of corrections that are greatly appreciated. We are grateful to Y Aikawa, A Bachmann, P Caselli, D Galli, P Goldsmith, D Johnstone, C Lada, C Román-Zúñiga,

S Schnee, F van der Tak, and C Vastel for supplying figures or material for figures prior to or post-publication. We are also grateful to members of the c2d team who provided information well in advance of publication, in particular, to N Evans, T Bourke, M Enoch, and M Dunham. EAB's work has been supported by the National Science Foundation under Grant No. 0335207, and MT's work has been partly supported by project AYA 2003-07584 from the Spanish Ministerio de Educación y Ciencia.

References

- Aikawa Y, Herbst E, Roberts H, Caselli P. 2005. *Astrophys. J.* 620:330
- Aikawa Y, Ohashi N, Inutsuka SI, Herbst E, Takakuwa S. 2001. *Astrophys. J.* 552:639
- Allen L, Megeath T, Gutermuth R, Myers PC, Wolk S, et al. 2007 In *Protostars and Planets V*, ed. B Reipurth, D Jewitt, K Keils, p. 361. Tucson: Univ. Ariz.
- Alves JF, Lada CJ, Lada EA. 1999. *Astrophys. J.* 515:265
- Alves JF, Lada CJ, Lada EA. 2001. *Nature* 409:159
- André P, Bouwman J, Belloche A, Hennebelle P. 2003. In *Chemistry as a Diagnostic of Star Formation*, ed. CL Curry, M Fich, p. 127. Ottawa: NRC Press
- André P, Ward-Thompson D, Motte F. 1996. *Astron. & Astrophys.* 314:625
- Arce HG, Goodman AA, Bastien P, Manset N, Sumner M. 1998 *Astrophys. J. Letters* 499:L93
- Arons J, Max CE. 1975. *Astrophys. J. Letters* 196:L77
- Arquilla R, Goldsmith PF. 1986. *Astrophys. J.* 303:356
- Bacmann A, André P, Puget JL, Abergel A, Bontemps S, Ward-Thompson D. 2000. *Astron. & Astrophys.* 361:555
- Bacmann A, Lefloch B, Ceccarelli C, Castets A, Steinacker J, Loinard L. 2002. *Astron. & Astrophys.* 389:L6
- Bacmann A, Lefloch B, Ceccarelli C, Steinacker J, Castets A, Loinard L. 2003. *Astrophys. J. Letters* 585:L55
- Ballesteros-Paredes J, Klessen RS, Vázquez-Semadeni E. 2003. *Astrophys. J.* 592:188
- Ballesteros-Paredes J, Klessen RS, Mac Low MM, Vázquez-Semadeni E. 2007. In *Protostars and Planets V*, ed. B Reipurth, D Jewitt, K Keils. p. 63. Tucson: Univ. Ariz.
- Ballesteros-Paredes J, Vázquez-Semadeni E, Scalo J. 1999. *Astrophys. J.* 515:286
- Bally J, Stark AA, Wilson RW, Langer WD. 1987, *Astrophys. J. Letters* 312:L45
- Barnard EE. 1907. *Astrophys. J.* 25:218
- Barnard EE. 1919. *Astrophys. J.* 49:1-24
- Barnard EE. 1927. *Catalogue of 349 dark objects in the sky*. Chicago:University of Chicago Press
- Basu S, Mouschovias TC. 1994. *Astrophys. J.* 432:720
- Basu S. 2000. *Astrophys. J. Letters* 540:L103

- Bazell D, Desert FX. 1988. *Astrophys. J.* 333:353
- Beech M. 1987. *Astrophys. Space Sci.* 133:193
- Beech M. 1992. *Astrophys. Space Sci.* 192:103
- Beichman CA, Myers PC, Emerson JP, Harris S, Mathieu R, et al. 1986. *Astrophys. J.* 307:337
- Benson PJ, Myers PC. 1989. *Astrophys. J. Suppl.* 71:89
- Bergin EA, Langer, WD. 1997. *Astrophys. J.* 486:316
- Bergin EA, et al. 2000. *Astrophys. J. Letters* 539:L129
- Bergin EA, Alves J, Huard T, Lada CJ. 2002. *Astrophys. J. Letters* 570:L101
- Bergin EA, Snell RL. 2002. *Astrophys. J. Letters* 581:L105
- Bergin EA, Hartmann LW, Raymond JC, Ballesteros-Paredes J. 2004. *Astrophys. J.* 612:921
- Bergin EA, Melnick GJ, Gerakines PA, Neufeld DA, Whittet DCB. 2005. *Astrophys. J. Letters* 627:L33
- Bergin EA, Maret S, van der Tak FFS, Alves J, Carmody SM, Lada CJ. 2006. *Astrophys. J.* 645:369
- Bernes C. 1979. *Astron. & Astrophys.* 73:67
- Bianchi S, Gonçalves J, Albrecht M, Caselli P, Chini R, et al. 2003. *Astron. & Astrophys.* 399:L43
- Bisschop, SE, Fraser HJ, Öberg KI, van Dishoeck EF, Schlemmer S. 2006. *Astron. & Astrophys.* 449:1297
- Blitz, L. 1993, In *Protostars and Planets III*, ed. EH Levy, JI Lunine, p. 125. Tucson: Univ. Ariz.
- Blitz L, Shu FH. 1980. *Astrophys. J.* 238:148
- Blitz L, Williams JP. 1997. *Astrophys. J. Letters* 488:L145
- Bodenheimer P. 1995. *Ann. Rev. Astron. Astrophys.* 33:199
- Bohlin RC, Savage, BD, Drake JF. 1978. *Astrophys. J.* 224:132
- Bok BJ. 1948. *Centennial Symposia, Harvard Obs. Monograph No. 7*, 53
- Bok BJ. 1977. *Pub. Astron. Soc. Pacific* 89:597
- Bok BJ, Reilly EF. 1947. *Astrophys. J.* 105:255
- Bonnell IA, Bate MR. 2006. *MNRAS* 370:488
- Bonnor WB. 1956. *MNRAS* 116:351
- Bourke TL, Myers PC, Robinson G, Hyland AR. 2001. *Astrophys. J.* 554:916
- Bringa EM, Johnson RE. 2004. *Astrophys. J.* 603:159
- Brunt CM, Heyer MH. 2002. *Astrophys. J.* 566:289
- Brunt CM, Mac Low MM. 2004. *Astrophys. J.* 604:196
- Burke JR, Hollenbach DJ. 1983. *Astrophys. J.* 265:223
- Burkert A, Hartmann L. 2004. *Astrophys. J.* 616:288
- Cambrésy L. 1999. *Astron. & Astrophys.* 345:965
- Cambrésy L, Beichman CA, Jarrett TH, Cutri RM. 2002. *Astron. J.* 123:2559

- Carey SJ, Clark FO, Egan MP, Price SD, Shipman RF, Kuchar TA. 1998. *Astrophys. J.* 508:721
- Caselli P, Walmsley CM, Terzieva R, Herbst E. 1998. *Astrophys. J.* 499:234
- Caselli P, Walmsley CM, Tafalla M, Dore L, Myers PC. 1999. *Astrophys. J. Letters* 523:L165
- Caselli P, Benson PJ, Myers PC, Tafalla M. 2002. *Astrophys. J.* 572:238
- Caselli P, Walmsley CM, Zucconi A, Tafalla M, Dore L, Myers PC. 2002. *Astrophys. J.* 565:331
- Caselli P, Walmsley CM, Zucconi A, Tafalla M, Dore L, Myers PC. 2002. *Astrophys. J.* 565:344
- Caselli P, van der Tak FFS, Ceccarelli C, Bacmann A. 2003. *Astron. & Astrophys.* 403:L37
- Ceccarelli C, Caselli P, Herbst E, Tielens AGGM, Caux E. 2007. In *Protostars and Planets V*, ed. B Reipurth, D Jewitt, K Keils. p. 47. Tucson: Univ. Ariz.
- Chandler, CJ, Carlstrom JE. 1996. *Astrophys. J.* 466:338
- Chandrasekhar S, Fermi E. 1953. *Astrophys. J.* 118:113
- Charnley SB, Tielens AGGM, Rodgers SD 1997. *Astrophys. J. Letters* 482:L203
- Charnley SB, Rodgers SD, Ehrenfreund P. 2001. *Astron. & Astrophys.* 378:1024
- Ciolek GE, Basu S. 2000. *Astrophys. J.* 529:925
- Ciolek GE, Mouschovias TC. 1998. *Astrophys. J.* 504:280
- Clemens DP, Barvainis R. 1988. *Astrophys. J. Suppl.* 68:257
- Collings MP, McCoustra MRS. 2005. *Astrochemistry: Recent Successes and Current Challenges*, ed. DC Lis, GA Blake, E Herbst, IAU Symposium. 231:405. Cambridge:Cambridge University Press
- Collings MP, Dever JW, Fraser HJ, McCoustra MRS. 2003. *Astrophys. Space Sci.* 285:633
- Crutcher RM. 1999. *Astrophys. J.* 520:706
- Crutcher RM, Nutter DJ, Ward-Thompson D, Kirk JM. 2004. *Astrophys. J.* 600:279
- Crutcher RM, Troland TH, Goodman AA, Heiles C, Kazes I, Myers PC. 1993. *Astrophys. J.* 407:175
- Crutcher RM, Troland TH. 2000. *Astrophys. J. Letters* 537:L139
- Dame TM, Hartmann D, Thaddeus P. 2001. *Astrophys. J.* 547:792
- Daniel F, Dubernet ML, Meuwly M, Cernicharo J, Pagani L. 2005. *MNRAS* 363:1083
- Davis LJ, Greenstein JL. 1951. *Astrophys. J.* 114:206
- del Burgo C, Laureijs RJ. 2005. *MNRAS* 360:901
- Di Francesco J, Evans NJ II, Caselli P, Myers PC, Shirley Y, et al. 2007. In *Protostars and Planets V*, ed. B Reipurth, D Jewitt, K Keils. p. 17. Tucson: Univ. Ariz.
- Dobashi K, Uehara H, Kandori R, Sakurai T, Kaiden M, et al. 2005. *PASJ* 57:1
- Dubernet ML, Grosjean A. 2002. *Astron. & Astrophys.* 390:793

- Ebert R. 1955. *Zeitschrift fur Astrophysik* 37:217
- Egan MP, Shipman RF, Price SD, Carey SJ, Clark FO, Cohen M 1998. *Astrophys. J. Letters* 494:L199
- Ehrenfreund, P. and S. B. Charnley 2000. *Ann. Rev. Astron. Astrophys.* . 38:427
- Elmegreen BG. 2000. *Astrophys. J.* 530:277
- Elmegreen BG. 2002. *Astrophys. J.* 564:773
- Elmegreen BG, Falgarone E. 1996. *Astrophys. J.* 471:816
- Elmegreen BG, Scalo J. 2004. *Ann. Rev. Astron. Astrophys.* 42:211
- Enoch ML, Young KE, Glenn J, Evans NJ II, Golwala S, et al. 2006. *Astrophys. J.* 638:293
- Evans NJ II. 1999. *Ann. Rev. Astron. Astrophys.* 37:311
- Evans NJ II, Rawlings JMC, Shirley YL, Mundy LG. 2001. *Astrophys. J.* 557:193
- Evans NJ II, Allen LE, Blake GA, Boogert ACA, Bourke T, et al. 2003. *Pub. Astron. Soc. Pacific* 115:965
- Falgarone E, Phillips TG, Walker CK. 1991. *Astrophys. J.* 378:186
- Falgarone E, Panis JF, Heithausen A, Perault M, Stutzki J, et al. 1998. *Astron. & Astrophys.* 331:669
- Florescu-Mitchell AI, Mitchell JBA. 2006. *Phys. Rep.* 430:277
- Flower DR, Pineau Des Forêts G, Walmsley CM 2006. *Astron. & Astrophys.* 449:621
- Flower DR, Pineau Des Forêts G, Walmsley CM. 2005. *Astron. & Astrophys.* 436:933
- Flower DR. 2001. *J. Phys. B At. Mol. Phys.* 34:2731
- Fraser HJ, Collings MP, McCoustra MRS, Williams DA. 2001. *MNRAS* 327:1165
- Frerking MA, Langer WD, Wilson RW. 1982. *Astrophys. J.* 262:590
- Galli D, Walmsley M, Gonçalves J. 2002. *Astron. & Astrophys.* 394:275
- Gammie CF, Ostriker EC. 1996. *Astrophys. J.* 466:814
- Garay G, Lizano S. 1999. *Pub. Astron. Soc. Pacific* 111:1049
- Geppert WD, Thomas R, Semaniak J, Ehlerding A, Millar TJ, et al. *Astrophys. J.* 609:459
- Gerlich D, Herbst E, Roueff E. 2002. *Plan. Space Sci.* 50:1275
- Gibb EL, Whittet DCB, Boogert ACA, Tielens AGGM. 2004. *Astrophys. J. Suppl.* 151:35
- Gillett FC, Forrest WJ. 1973. *Astrophys. J.* 179:483
- Goldsmith PF, Langer WD. 1978. *Astrophys. J.* 222:881
- Goldsmith PF. 1987. In *Interstellar Processes*, ed. DJ Hollenbach, HA Thronson, p. 51, Dordrecht: Reidel
- Goldsmith PF. 2001. *Astrophys. J.* 557:736
- Goldsmith PF, Li D. 2005. *Astrophys. J.* 622:938
- Goldsmith PF, Tang Y, Heyer M, Narayanan G, Snell R, et al. 2005. *BAAS* 37:1305

- Gonçalves J, Galli D, Walmsley M. 2004. *Astron. & Astrophys.* 415:617
- Goodman AA, Bastien P, Menard F, Myers PC. 1990. *Astrophys. J.* 359:363
- Goodman AA, Benson PJ, Fuller GA, Myers PC. 1993. *Astrophys. J.* 406:528
- Goodman AA, Jones TJ, Lada EA, Myers PC. 1995. *Astrophys. J.* 448:748
- Goodman AA, Barranco JA, Wilner DJ, Heyer MH. 1998. *Astrophys. J.* 504:223
- Gregersen EM, Evans NJ II. 2000. *Astrophys. J.* 538:260
- Guelin M, Langer WD, Wilson RW. 1982. *Astron. & Astrophys.* 107:107
- Hartmann L, Ballesteros-Paredes J, Bergin EA. 2001. *Astrophys. J.* 562:852
- Hartmann L. 2002. *Astrophys. J.* 578:914
- Hartmann L. 2003. *Astrophys. J.* 585:398
- Hasegawa TI, Herbst E. 1993. *MNRAS* 261:83
- Heiles C, Katz G. 1976. *Astron. J.* 81:37
- Heiles C, Goodman AA, McKee CF, Zweibel EG. 1993. In *Protostars and Planets III*, ed. EH Levy, JI Lunine, p. 279. Tucson: Univ. Ariz.
- Heiles C, Crutcher R. 2005. In *Cosmic Magnetic Fields*, ed. R Wielebinski, R Beck, p. 137. Berlin: Springer
- Hennebelle P, Pérault M, Teyssier D, Ganesh S. 2001. *Astron. & Astrophys.* 365:598
- Henning T, Wolf S, Launhardt R, Waters R. 2001. *Astrophys. J.* 561:871
- Herbst E. 2005. *J. Phys. Conf. Series* 4:17
- Herbst E, Chang Q, Cuppen HM. 2005. *J. Phys. Conf. Series* 6:18
- Herschel W. 1785. *Philosophical Transactions Series I* 75:213
- Heyer MH, Brunt CM. 2004. *Astrophys. J.* 615:L45
- Heyer MH, Vrba FJ, Snell RL, Schloerb FP, Strom SE, et al. 1987. *Astrophys. J.* 321:855
- Heyer MH, Schloerb FP. 1997. *Astrophys. J.* 475:173
- Heyer MH, Brunt C, Snell RL, Howe JE, Schloerb FP, et al. 1998. *Astrophys. J. Suppl.* 115:241
- Hirahara Y, Suzuki H, Yamamoto S, Kawaguchi K, Kaifu N, et al. 1992. *Astrophys. J.* 394:539
- Hirota, T., H. Maezawa, and S. Yamamoto 2004. *Astrophys. J.* . 617:399
- Hirota T, Ito T, Yamamoto S. 2002. *Astrophys. J.* 565:359
- Hjalmarson Å, et al. 2005. *Advances in Space Research* 36:1031
- Hornekær L, Baurichter A, Baouche S, Field D, Luntz AC 2003. *Science* 302:1943
- Houde M, Dowell CD, Hildebrand RH, Dotson JL, Vaillancourt JE, et al. 2004. *Astrophys. J.* 604:717
- Houghton HE. 1942. *Monthly Notes of the Astronomical Society of South Africa* 1:107
- Irvine WM, Goldsmith PF, Hjalmarson Å. 1987. In *Interstellar Processes*, ed. DJ Hollenbach, HA Thronson, ASSL 134:561. Dordrecht:Reidel

- Jackson JM, Rathborne JM, Shah RY, Simon R, Bania TM, et al. 2006. *Astrophys. J. Suppl.* 163:145
- Jappsen AK, Klessen RS. 2004. *Astron. & Astrophys.* 423:1
- Jijina J, Myers PC, Adams FC. 1999. *Astrophys. J. Suppl.* 125:161
- Johnstone D, Bally J. 1999. *Astrophys. J. Letters* 510:L49
- Johnstone D, Wilson CD, Moriarty-Schieven G, Joncas G, Smith G, et al. 2000. *Astrophys. J.* 545:327
- Johnstone D, Fich M, Mitchell GF, Moriarty-Schieven G. 2001. *Astrophys. J.* 559:307
- Johnstone D, Fiege JD, Redman RO, Feldman PA, Carey SJ. 2003. *Astrophys. J. Letters* 588:L37
- Johnstone D, Di Francesco J, Kirk H. 2004. *Astrophys. J. Letters* 611:L45
- Jones CE, Basu S, Dubinski J. 2001. *Astrophys. J.* 551:387
- Jørgensen JK, Schöier FL, van Dishoeck EF 2004 *Astron. & Astrophys.* 416:603
- Kandori R, Nakajima Y, Tamura M, Tatematsu K, Aikawa Y, et al. 2005. *Astron. J.* 130:2166
- Katz N, Furman I, Biham O, Pirronello V, Vidali G. 1999. *Astrophys. J.* 522:305
- Keto E, Broderick A, Lada CJ, Narayan R. 2006. *Astrophys. J.* 652:1366
- Kirk JM, Ward-Thompson D, André P. 2005. *MNRAS* 360:1506
- Kirk JM, Ward-Thompson D, Crutcher RM. 2006. *MNRAS* 369:1445
- Klessen RS, Ballesteros-Paredes J. 2004. *Baltic Astronomy* 13:365
- Koyama H, Inutsuka SI. 2000. *Astrophys. J.* 532:980
- Kuiper TBH, Langer WD, Velusamy T. 1996. *Astrophys. J.* 468:761
- Kramer C, Stutzki J, Rohrig R, Corneliussen U. 1998. *Astron. & Astrophys.* 329:249
- Kramer C, Alves J, Lada CJ, Lada EA, Sievers A, et al. 1999. *Astron. & Astrophys.* 342:257
- Kramer C, Richer J, Mookerjee B, Alves J, Lada C. 2003. *Astron. & Astrophys.* 399:1073
- Krumholz MR, McKee CF, Klein RI. 2005. *Nature* 438:332
- Lacy JH, et al. 1984. *Astrophys. J.* 276:533
- Langer WD, van Dishoeck EF, Bergin EA, Blake GA, Tielens AGGM, et al. 2000. In *Protostars and Planets IV*, ed. V Mannings, A Boss, SS Russell, p. 29. Tucson: Univ. of Arizona Press
- Lada EA, Strom KM, Myers PC. 1993. In *Protostars and Planets III*, ed. EH Levy, JI Lunine, p. 245. Tucson: Univ. Ariz.
- Lada CJ, Lada EA, Clemens DP, Bally J. 1994. *Astrophys. J.* 429:694
- Lada CJ, Alves J, Lada EA. 1999. *Astrophys. J.* 512:250
- Lada CJ, Bergin EA, Alves JF, Huard TL. 2003. *Astrophys. J.* 586:286
- Lada CJ, Alves JF, Lombardi M. 2007, In *Protostars and Planets V*, ed. B Reipurth, D Jewitt, K Keils. p. 3. Tucson: Univ. Ariz.

- Larson RB. 1969. *MNRAS* 145:271
- Larson RB. 1981. *MNRAS* 194:809
- Larson RB. 1995. *MNRAS* 272:213
- Larson RB. 2002. *MNRAS* 332:155
- Larson RB. 2003. *Rep. Prog. Phys.* 66:1651
- Lazarian A, Goodman AA, Myers PC. 1997. *Astrophys. J.* 490:273
- Lazarian A, Pogosyan D. 2000. *Astrophys. J.* 537:720
- Lee CW, Myers PC, Tafalla M. 1999. *Astrophys. J.* 526:788
- Lee CW, Myers PC, Tafalla M. 2001. *Astrophys. J. Suppl.* 136:703
- Lee JE, Bergin EA, Evans NJ II. 2004. *Astrophys. J.* 617:360
- Leger A, Jura M, Omont A. 1985 *Astron. & Astrophys.* . 144:147
- Lehtinen K, Mattila K, Lemke D, Juvela M, Prusti T, Laureijs R. 2003. *Astron. & Astrophys.* 398:571
- Leung CM, Brown RL. 1977. *Astrophys. J. Letters* 214:L73
- Levin SM, Langer WD, Velusamy T, Kuiper TBH, Crutcher RM. 2001. *Astrophys. J.* 555:850
- Li ZY, Shematovich VI, Wiebe DS, Shustov BM. 2002. *Astrophys. J.* 569:792
- Linsky JL, et al. 2006. *Astrophys. J.* 647:1106
- Lis DC, E. Roueff, Gerin M, Phillips TG, Coudert LH, et al. 2002. *Astrophys. J. Letters* 571:L55
- Lizano S, Shu FH. 1989. *Astrophys. J.* 342:834
- Lombardi M, Alves J. 2001. *Astron. & Astrophys.* 377:1023
- Lombardi M, Alves J, Lada CJ. 2006. *Astron. & Astrophys.* 454:781
- Loren RB. 1989. *Astrophys. J.* 338:925
- Lovejoy S. 1983. *Science* 216:185
- Maret S, Bergin EA, Lada CJ. 2006. *Nature* 442:425
- Mac Low MM, Klessen RS, Burkert A, Smith MD. 1998. *Phys. Rev. Lett.* 80:2754
- Mac Low MM, Klessen RS. 2004. *Rev. Mod. Phys.* 76:125
- Mandelbrot BB. 1983, *The Fractal Geometry of Nature*. New York: Springer
- Mathis JS, Mezger PG, Panagia N. 1983. *Astron. & Astrophys.* 128:212
- Matthews BC, Wilson CD. 2000. *Astrophys. J.* 531:868
- Matthews BC, Wilson CD, Fiege JD. 2001. *Astrophys. J.* 562:400
- McKee CF. 1989. *Astrophys. J.* 345:782
- McKee CF, Zweibel EG, Goodman AA, Heiles C. 1993. In *Protostars and Planets III*, ed. EH Levy, JI Lunine, p. 327. Tucson: Univ. Ariz.
- McKee CF. 1999. In *The Origin of Stars and Planetary Systems*, ed. CL Lada, D. Kylafis, p. 29. Dordrecht: Kluwer
- McLaughlin DE, Pudritz RE. 1996. *Astrophys. J.* 469:194
- Melnick GJ, Bergin EA. 2005. *Advances in Space Research* 36:1027
- Mestel L, Spitzer L Jr. 1956. *MNRAS* 116:503

- Mezger PG, Sievers AW, Haslam CGT, Kreysa E, Lemke R, et al. 1992. *Astron. & Astrophys.* 256:631
- Miesch MS, Scalo J, Bally J. 1999. *Astrophys. J.* 524:895
- Millar TJ, Bennett A, Herbst E. 1989. *Astrophys. J.* 340:906
- Miller GE, Scalo JM. 1979. *Astrophys. J. Suppl.* 41:513
- Monet D. 1996. *BAAS* 28:905
- Moneti A, Pipher JL, Helfer HL, McMillan RS, Perry ML. 1984. *Astrophys. J.* 282:508
- Motte F, André P, Neri R. 1998. *Astron. & Astrophys.* 336:150
- Mouschovias TC. 1976. *Astrophys. J.* 207:141
- Mouschovias TC, Ciolek GE. 1999. In *The Origin of Stars and Planetary Systems*, ed. CL Lada, D. Kylafis, p. 305. Dordrecht: Kluwer
- Mouschovias TC, Paleologou EV. 1979. *Astrophys. J.* 230:204
- Mouschovias TC, Tassis K, Kunz MW. 2006. *Astrophys. J.* 646:1043
- Myers PC. 1983. *Astrophys. J.* 270:105
- Myers PC. 2005. *Astrophys. J.* 623:280
- Myers PC. 1995. In *Molecular Clouds and Star Formation*, eds. C Yuan, J You, p. 47. Singapore: World Scientific
- Myers PC, Benson PJ. 1983. *Astrophys. J.* 266:309
- Myers PC, Fuller GA, Mathieu RD, Beichman CA, Benson PJ, et al. 1987. *Astrophys. J.* 319:340
- Myers PC, Goodman AA. 1991. *Astrophys. J.* 373:509
- Myers PC, Fuller GA, Goodman AA, Benson PJ. 1991. *Astrophys. J.* 376:561
- Myers PC, Mardones D, Tafalla M, Williams JP, Wilner DJ. 1996. *Astrophys. J. Letters* 465:L133
- Myers PC, Evans NJ II, Ohashi N. 2000. In *Protostars and Planets IV*, ed. V Mannings, AP Boss, SS Russell, p. 217. Tucson: Univ. Ariz.
- Nagaoka A, Watanabe N, Kouchi A. 2005. *Astrophys. J. Letters* 624:L29
- Nakano T. 1998. *Astrophys. J.* 494:587
- Nakano T, Nakamura T. 1978. *Pub. Astron. Soc. Japan* 30:671
- Neufeld DA, Melnick GJ, Sonnentrucker P, Bergin EA, Green JD, et al. 2006. *Astrophys. J.* 649:816
- Öberg KI, van Broekhuizen F, Fraser HJ, Bisschop SE, van Dishoeck EF, Schlemmer S. 2005. *Astrophys. J. Letters* 621:L33
- Ossenkopf V, Henning T. 1994. *Astron. & Astrophys.* 291:943
- Ossenkopf V, Mac Low MM. 2002. *Astron. & Astrophys.* 390:307
- Osterbrock DE. 1961. *Astrophys. J.* 134:270
- Ostriker EC, Stone JM, Gammie CF. 2001. *Astrophys. J.* 546:980
- Padoan P, Juvela M, Goodman AA, Nordlund Å. 2001. *Astrophys. J.* 553:227
- Padoan P, Nordlund Å. 1999. *Astrophys. J.* 526:279

- Pagani L, Lagache G, Bacmann A, Motte F, Cambr  sy L, et al. 2003. *Astron. & Astrophys.* 406:L59
- Pagani L, Pardo JR, Apponi AJ, Bacmann A, Cabrit S. et al. 2005. *Astron. & Astrophys.* 429:181
- Palla F, Stahler SW. 2002. *Astrophys. J.* 581:1194
- Penston MV. 1969. *MNRAS* 144:425
- Perault M. et al. 1996. *Astron. & Astrophys.* 315:L165
- Pety J, Falgarone E. 2003. *Astron. & Astrophys.* 412:417
- Pereyra A, Magalh  es AM. 2004. *Astrophys. J.* 603:584
- Phillips TG, Vastel C. 2003. in *Chemistry as a Diagnostic of Star Formation*, eds CL Curry, M Fich. Ottawa:NRC Press, p. 3
- Pillai T, Wyrowski F, Carey SJ, Menten KM. 2006. *Astron. & Astrophys.* 450:569
- Pineau des Forets, G., Flower, D. R., & McCarroll, R. 1991, *MNRAS* , 248, 173
- Pontoppidan KM. 2006. *Astron. & Astrophys.* 453:L47
- Pontoppidan KM, van Dishoeck EF, Dartois E, Fraser HJ, Banhidi Z, J  rgensen JK, The C2d Team. 2005. *Astrochemistry: Recent Successes and Current Challenges*, ed. DC Lis, GA Blake, E Herbst, IAU Symposium. 231:114 Cambridge:Cambridge University Press
- Prantzos N, Aubert O. 1995. *Astron. & Astrophys.* 302:69
- Pratap P, Dickens JE, Snell RL, Miralles MP, Bergin EA. et al. 1997. *Astrophys. J.* 486:862
- Rachford BL, Snow TP, Tumlinson J, Shull MJ, Blair WP. et al. 2002. *Astrophys. J.* 577:221
- Ragan SE, Bergin EA, Plume R, Gibson DL, Wilner DJ, et al. 2006. *Astrophys. J. Suppl.* 166:567
- Rathborne JM, Jackson JM, Simon R. 2006. *Astrophys. J.* 641:389
- Rawlings JMC, Hartquist TW, Menten KM, Williams DA. 1992. *MNRAS* 255:471
- Rieke GH, Lebofsky MJ. 1985. *Astrophys. J.* 288:618
- Reipurth B. 1983. *Astron. & Astrophys.* 117:183
- Reipurth B, Jewitt D, Keil K. eds. 2007. *Protostars and Planets V*. Tucson, AZ: Univ. of Arizona Press
- Ridge NA, Di Francesco J, Kirk H, Li D, Goodman AA, et al. 2006. *Astron. J.* 131:2921
- Roberts H, Herbst E, Millar TJ 2003. *Astrophys. J. Letters* 591:L41
- Rodr  guez LF. 2005. In *The Cool Universe: Observing Cosmic Dawn*, ed. C Lidman, D Alloin, p. 146. San Francisco: ASP
- Rosolowsky EW, Goodman AA, Wilner DJ, Williams JP. 1999. *Astrophys. J.* 524:887
- Roueff E, Tin   S, Coudert LH, Pineau des For  ts G, Falgarone E, Gerin M. 2000. *Astron. & Astrophys.* 354:L63
- Rybicki GB, Hummer DG. 1991. *Astron. & Astrophys.* 245:171

- Ryden BS. 1996. *Astrophys. J.* 471:822
- Salpeter EE. 1955. *Astrophys. J.* 121:161
- Sánchez N, Alfaro EJ, Pérez E. 2005. *Astrophys. J.* 625:849
- Schnee S, Goodman A. 2005. *Astrophys. J.* 624:254
- Scalo J. 1990. In *Physical Processes in Fragmentation and Star Formation*, ed. R Capuzzo-Dolcetta, C Chiosi, A DiFazio, p. 151. Dordrecht: Kluwer
- Shen CJ, Greenberg, JM, Schutte WA, van Dishoeck EF. 2004. *Astron. & Astrophys.* 415:203
- Schneider S, Elmegreen BG. 1979. *Astrophys. J. Suppl.* 41:87
- Shinnaga H, Tsuboi M, Kasuga T. 1999. In *Proceedings of Star Formation 1999* ed. T Nakamoto, Nobeyama: Nobeyama Radio Observatory, p. 175
- Shu FH 1977. *Astrophys. J.* 214:488
- Shu FH, Adams FC, Lizano S. 1987. *Ann. Rev. Astron. Astrophys.* 25:23
- Simon M. 1997. *Astrophys. J. Letters* 482:L81
- Simon R, Jackson JM, Rathborne JM, Chambers ET. 2006. *Astrophys. J.* 639:227
- Skrutskie MF, Cutri RM, Stiening R, Weinberg MD, Schneider S, et al. 2006. *Astron. J.* 131:1163
- Snell RL. 1981. *Astrophys. J. Suppl.* 45:121
- Snell RL., et al. 2000. *Astrophys. J. Letters* 539:L101
- Spitzer L Jr. 1978. *Physical Processes in the Interstellar Medium*. New York: Wiley
- Sridharan TK, Beuther H, Saito M, Wyrowski F, Schilke P. 2005. *Astrophys. J. Letters* 634:L57
- Stamatellos D, Whitworth AP. 2003. *Astron. & Astrophys.* 407:941
- Stamatellos D, Whitworth AP, André P, Ward-Thompson D. 2004. *Astron. & Astrophys.* 420:1009
- Stantcheva T, Herbst E. 2003. *MNRAS* 340:983
- Stark R, van der Tak FFS, & van Dishoeck, EF. 1999. *Astrophys. J. Letters* 521:L67
- Stepnik B, Abergel A, Bernard JP, Boulanger F, Cambrésy L, et al. 2003. *Astron. & Astrophys.* 398:551
- Stone JM, Ostriker EC, Gammie CF. 1998. *Astrophys. J. Letters* 508:L99
- Stutzki J, Bensch F, Heithausen A, Ossenkopf V, Zielinsky M. 1998. *Astron. & Astrophys.* 336:697
- Stutzki J, Güsten R. 1990. *Astrophys. J.* 356:513
- Suzuki H, Yamamoto S, Ohishi M, Kaifu N, Ishikawa SI, et al. 1992. *Astrophys. J.* 392:551
- Sun K, Kramer C, Ossenkopf V, Bensch F, Stutzki J, Miller M. 2006. *Astron. & Astrophys.* 451:539
- Swade DA. 1989. *Astrophys. J.* 345:828
- Tachihara K, Onishi T, Mizuno A, Fukui Y. 2002. *Astron. & Astrophys.* 385:909

- Tafalla M, Mardones D, Myers PC, Caselli P, Bachiller R, Benson PJ. 1998. *Astrophys. J.* 504:900
- Tafalla M, Myers PC, Caselli P, Walmsley CM, Comito C. 2002. *Astrophys. J.* 569:815
- Tafalla M, Myers PC, Caselli P, Walmsley CM. 2004. *Astron. & Astrophys.* 416:191
- Tafalla M, Santiago J. 2004. *Astron. & Astrophys.* 414:L53
- Tafalla M, Santiago J, Myers PC, Caselli P, Walmsley CM, Crapsi A. 2006. *Astron. & Astrophys.* 455:577
- Testi L, Sargent AI. 1998. *Astrophys. J. Letters* 508:L91
- Teyssier D, Hennebelle P, Pérault M. 2002. *Astron. & Astrophys.* 382:624
- Tielens AGGM, Hagen W. 1982. *Astron. & Astrophys.* 114:245
- Tielens AGGM. 1983. *Astron. & Astrophys.* 119:177
- Tielens AGGM. 2005. *The Physics and Chemistry of the Interstellar Medium*, Cambridge:Cambridge University Press
- Tomisaka K, Ikeuchi S, Nakamura T. 1988. *Astrophys. J.* 335:239
- Tóth LV, Haas M, Lemke D, Mattila K, Onishi T. 2004. *Astron. & Astrophys.* 420:533
- Troland TH, Crutcher RM, Goodman AA, Heiles C, Kazes I, Myers PC. 1996. *Astrophys. J.* 471:302
- Turner BE, Heiles C. 2006. *Astrophys. J. Suppl.* 162:388
- van der Tak FFS, Caselli P, Ceccarelli C. 2005. *Astron. & Astrophys.* 439:195
- van Dishoeck EF. 2004. *Ann. Rev. Astron. Astrophys.* 42:119
- van Dishoeck EF, Blake GA 1998. *Ann. Rev. Astron. Astrophys.* . 36:317
- Vastel C, Phillips TG, Yoshida H. 2004. *Astrophys. J. Letters* 606:L127
- Vazquez-Semadeni E. 1994. *Astrophys. J.* 423:681
- Vázquez-Semadeni E, Ballesteros-Paredes J, Klessen RS. 2003. *Astrophys. J. Letters* 585:L131
- Walsh AJ, Myers PC, Burton MG. 2004. *Astrophys. J.* 614:194
- Walmsley CM, Ungerechts H. 1983. *Astron. & Astrophys.* 122:164
- Walmsley CM, Flower DR, Pineau des Forêts G. 2004. *Astron. & Astrophys.* 418:1035
- Ward-Thompson D, André P, Crutcher R, Johnstone D, Onishi T, Wilson C. 2007. In *Protostars and Planets V*, ed. B Reipurth, D Jewitt, K Keils. p. 33. Tucson: Univ. Ariz.
- Ward-Thompson D, André P, Kirk JM. 2002. *MNRAS* 329:257
- Ward-Thompson D, Kirk JM, Crutcher RM, Greaves JS, Holland WS, André P. 2000. *Astrophys. J. Letters* 537:L135
- Ward-Thompson D, Motte F, André P. 1999. *MNRAS* 305:143
- Ward-Thompson D, Scott PF, Hills RE, André P. 1994. *MNRAS* 268:276
- Weingartner JC, Draine BT 2001. *Astrophys. J. Suppl.* 134:263

- Weinreb S, Barrett AH, Meeks ML, Henry JC 1963. *Nature* 200:829
- Werner M, Fazio G, Rieke G, Roellig TL, Watson DM. 2006. *Ann. Rev. Astron. Astrophys.* 44:269
- Whittet DCB, Bode MF, Longmore AJ, Adamson AJ, McFadzean AD, et al. 1988. *MNRAS* 233:321
- Whittet DCB, Gerakines PA, Hough JH, Shenoy SS. 2001. *Astrophys. J.* 547:872
- Whittet DCB, Shenoy SS, Bergin EA, Chiar JE, Gerakines PA, et al. 2007. *Astrophys. J.* 655:332
- Whitworth AP, Ward-Thompson D. 2001. *Astrophys. J.* 547:317
- Willacy K, Langer WD, Velusamy T. 1998. *Astrophys. J. Letters* 507:L171
- Williams JP, de Geus EJ, Blitz L. 1994. *Astrophys. J.* 428:693
- Williams JP, Bergin EA, Caselli P, Myers PC, Plume R. 1998. *Astrophys. J.* 503:689
- Williams JP, Blitz L, McKee CF. 2000. In *Protostars and Planets IV*, ed. V Mannings, A Boss, SS Russell, p. 97. Tucson: Univ. of Arizona Press
- Williams JP, Myers PC, Wilner DJ, di Francesco J. 1999. *Astrophys. J. Letters* 513:L61
- Wilson RW, Jefferts KB, Penzias AA. 1970. *Astrophys. J. Letters* 161:L43
- Wolf M. 1923. *Astronomische Nachrichten* 219: 109
- Wolf S, Launhardt R, Henning T. 2003. *Astrophys. J.* 592:233
- Young CH, Jørgensen JK, Shirley YL, Kauffmann J., Huard T, et al. 2004. *Astrophys. J. Suppl.* 154:396
- Young KE, Enoch ML, Evans NJ II, Glenn J, Sargent A, et al. 2006. *Astrophys. J.* 644:326
- Yun JL, Clemens DP. 1990. *Astrophys. J. Letters* 365:L73
- Zhou S, Wu Y, Evans NJ II, Fuller GA, Myers PC. 1989. *Astrophys. J.* 346:168
- Zucconi A, Walmsley CM, Galli D. 2001. *Astron. & Astrophys.* 376:650
- Zuckerman B, Evans NJ II. 1974. *Astrophys. J. Letters* 192:L149

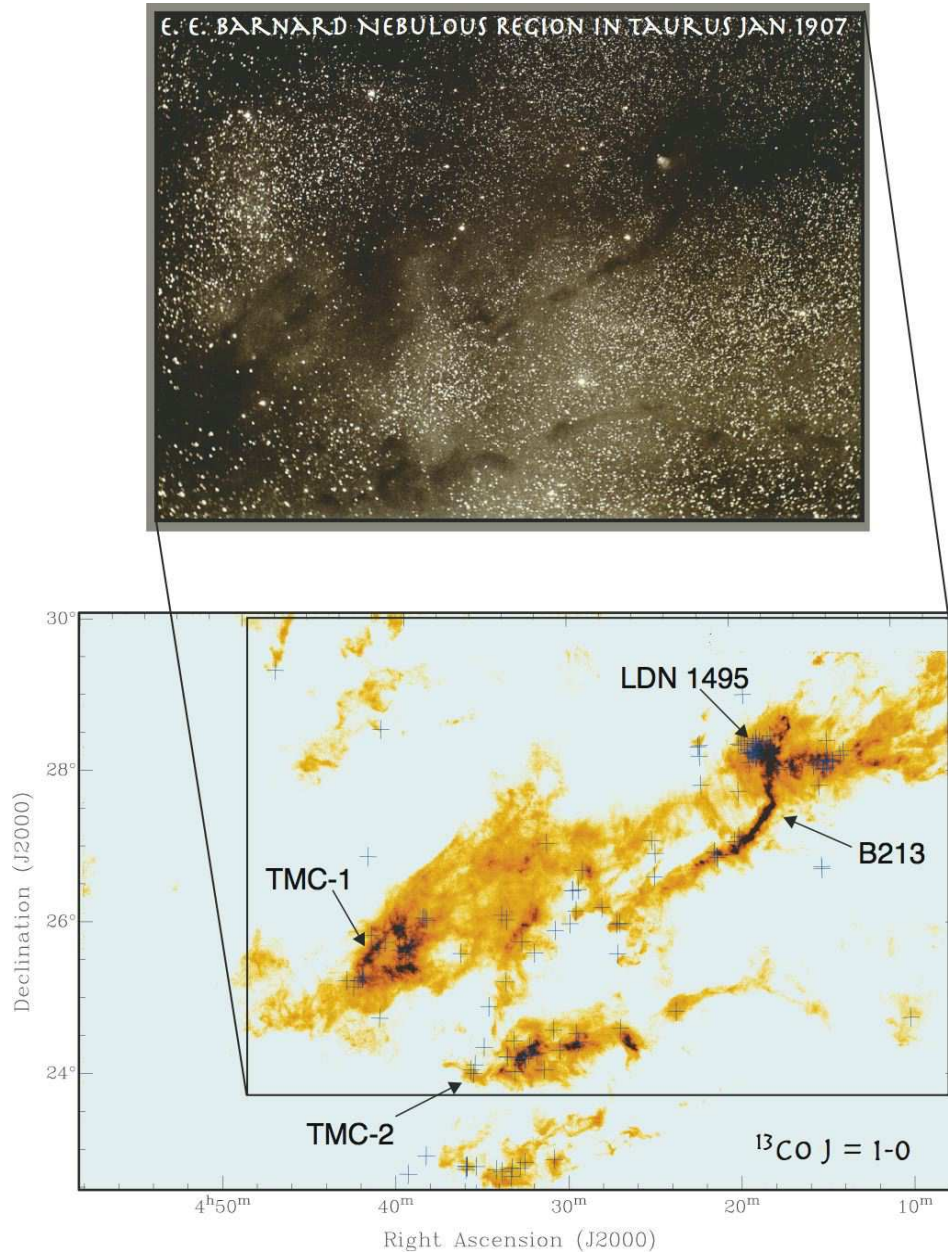


Figure 1: *Top Panel:* Photographic image of the Taurus Molecular Cloud taken by E. E. Barnard (Barnard 1919). His notes state that, “*very few regions of the sky are so remarkable as this one. Indeed the photograph is one of the most important of the collection, and bears the strongest proof of the existence of obscuring matter in space*”. Courtesy of the Observatories of the Carnegie Institution of Washington. *Bottom Panel:* $^{13}\text{CO } J=1-0$ integrated emission map of the same region obtained using the Five College Radio Astronomy Observatory. Crosses mark the location of known protostellar objects and the emission color scale ranges from 0.5 – 10 K km s⁻¹. Image kindly provided by PF Goldsmith in advance of publication.

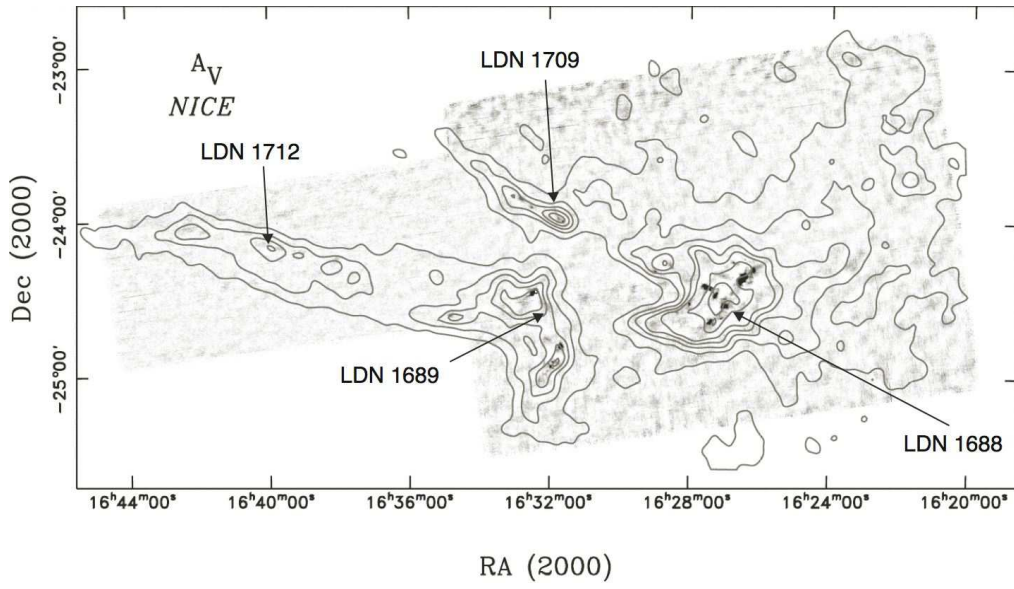


Figure 2: Maps of IR extinction (contours) and submm emission (greyscale) for the ρ Ophiuchus dark cloud illustrating how the dense gas, responsible for the submm continuum emission, represents a small fraction of the total amount (and an even smaller fraction of the total volume). Most of the gas in the cloud is in the form of low density, low extinction gas. Contours are at $A_V = 2, 4, 6, 8, 10, 15,$ and 20 mag with an effective resolution of $5'$. Figure from Young et al. (2006).

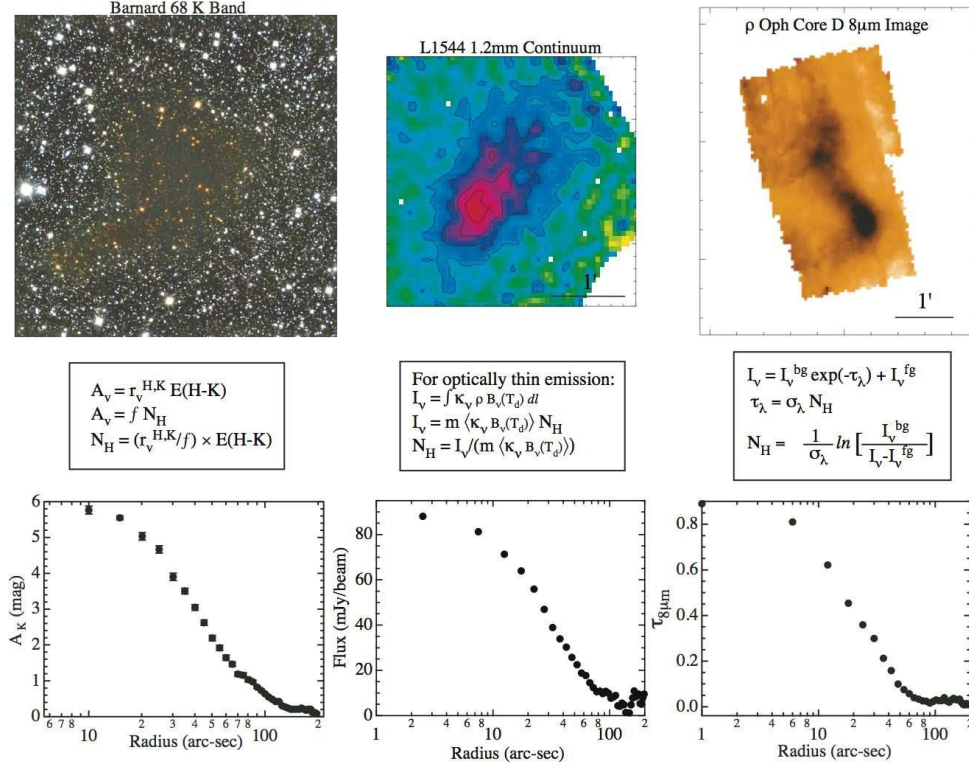


Figure 3: Figure illustrating the various methods used to determine the column and volume density of starless molecular cores. *Left Panels:* K-band image of Barnard 68 and plot of the derived A_K with $10''$ resolution as a function of core radius (taken from Alves, Lada & Lada (2001) with A_K vs. radius provided by C Román-Zúñiga. In this method the measured quantity is the H–K excess which is related to A_V by the extinction law, parameterized by $r_v^{H,K}$. A_V is correlated to the hydrogen column from UV line measurements, parameterized by f (Bohlin et al. 1978; Rachford et al. 2002). *Middle Panels:* 1.2 mm dust continuum emission map and flux vs. radius for L1544 (taken from Ward-Thompson, Motte & André 1999 and Tafalla et al. 2002). κ_ν is the dust opacity per unit gas mass, ρ is the dust density, and m the hydrogen mass (corrected for He). *Right Panels:* 7 μ m ISOCAM image and opacity vs. radius for ρ Oph D (taken from Bacmann et al. 2000). At 7 μ m the emission from polycyclic aromatic hydrocarbons (PAHs) provides a bright background and the dense core appears in absorption. In this method the absorbing opacity is related to the hydrogen column via the dust absorption cross-section, σ_λ .

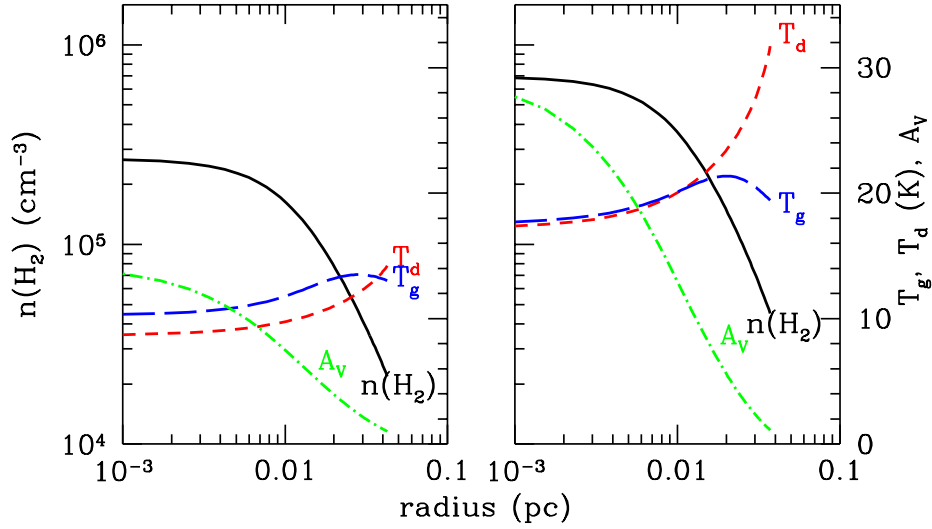


Figure 4: Left: Molecular hydrogen density, n_{H_2} , gas (T_g) and dust (T_d) temperatures, and visual extinction (A_V) as a function of radius for a marginally stable spherical cloud with $M = 1 M_\odot$ exposed to the standard interstellar radiation field ($G_0 = 1$). Right: Same as *left* but for a marginally stable cloud ($M = 1.6 M_\odot$) bounded by an external pressure ($p_{\text{ext}} = 10^6 \text{ cm}^{-3} \text{ K}$) and illuminated by an enhanced radiation field ($G_0 = 10$). Figure taken from Galli, Walmsley & Gonçalves (2002).

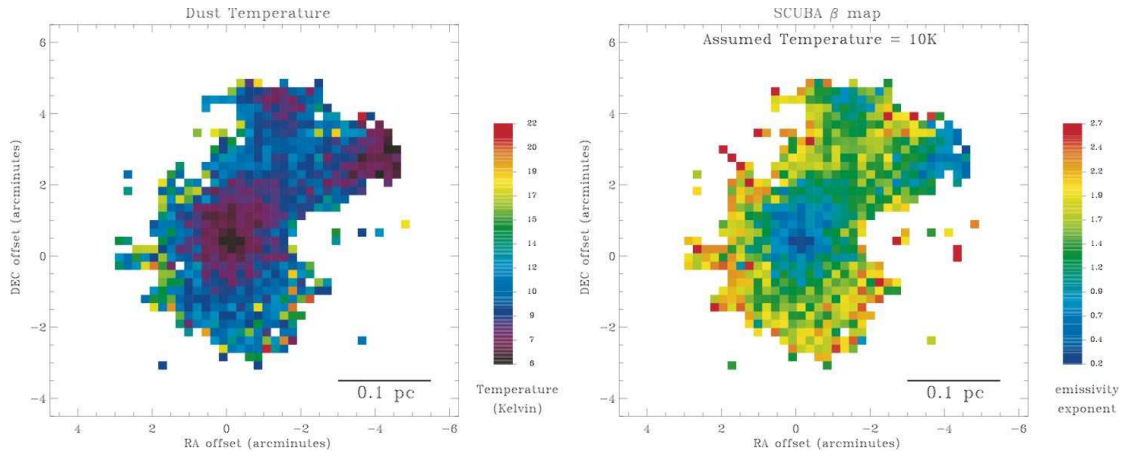


Figure 5: *Right:* Map of dust temperature in TMC-1C derived from 450 and 850 μm SCUBA maps assuming dust emissivity index $\beta = 1.5$. *Left:* Map of dust emissivity index, β in TMC-1C assuming a constant temperature of 10 K. Taken from Schnee & Goodman (2005).

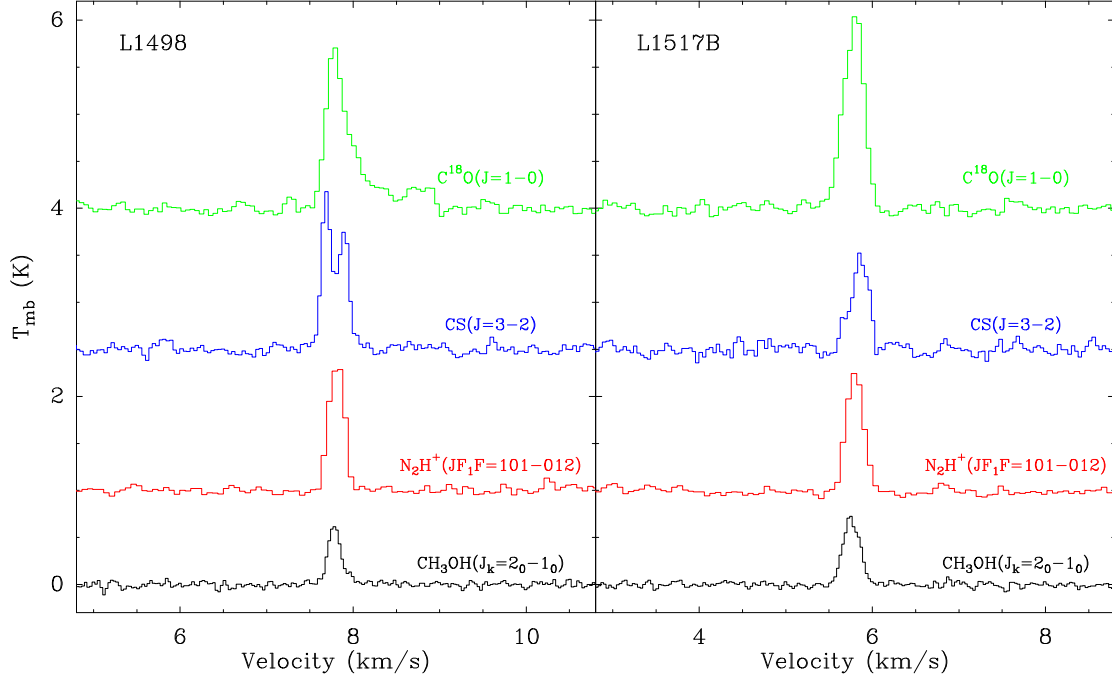


Figure 6: Sample spectra from the starless cores L1498 and L1517B in the Taurus-Auriga dark cloud illustrating the variety of shapes and intensities commonly observed. The C^{18}O spectra trace both dense and low-density gas (due to the low dipole moment of the molecule), and often present additional velocity components from unrelated gas that moves at velocities of the order of 1 km s^{-1} (red gas in L1498). The optically thick CS spectra are sensitive to the relative motions of the core and its envelope thanks to the presence of self-absorptions, that commonly indicate inward (L1498) or outward (L1517B) motions at the level of 0.1 km s^{-1} . The optically thin N_2H^+ and CH_3OH lines trace different regions of the core depending on their chemistry, and their narrow linewidths reveal the subsonic nature of the gas internal motions. Data from Tafalla et al. (2004) and Tafalla et al. (2006).

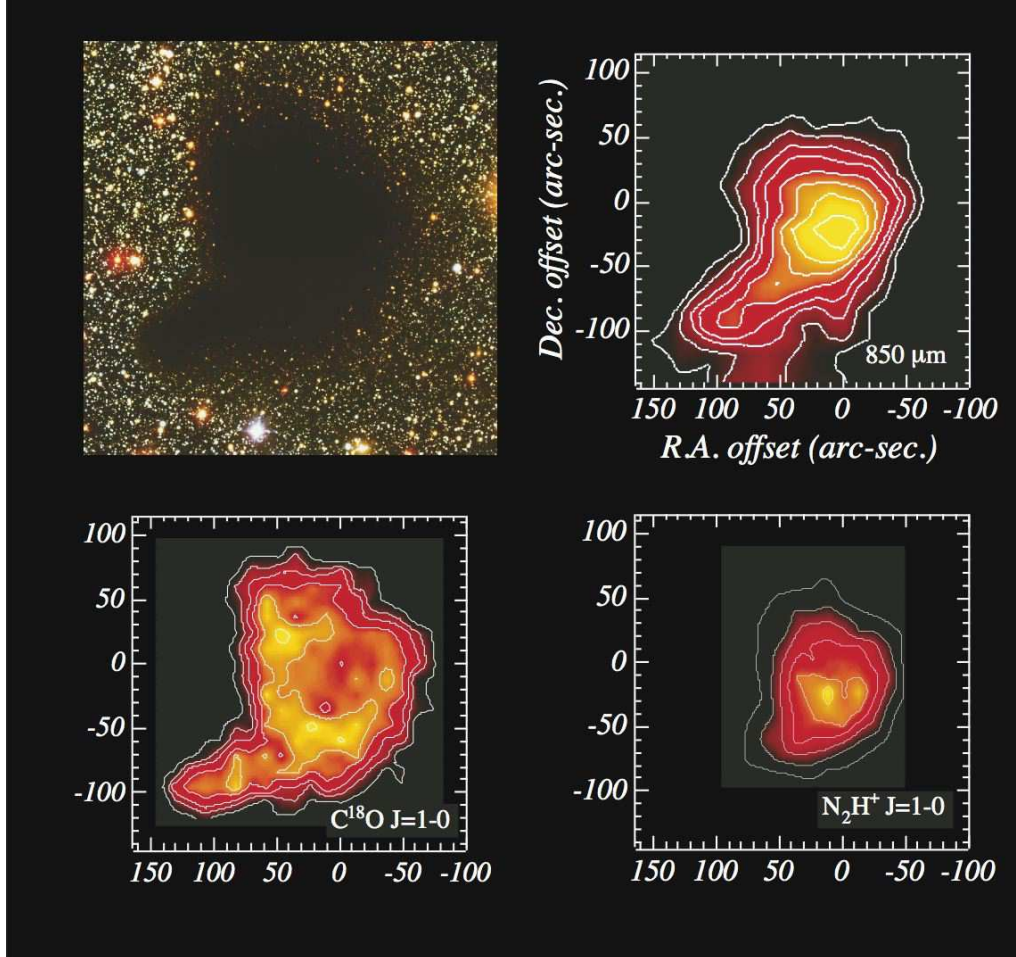


Figure 7: A deep optical image of the dark globule Barnard 68 (*top left*; Alves, Lada & Lada 2001) along with contour maps of integrated intensity from molecular emission lines of N_2H^+ (contour levels: 0.3–1.8 by 0.3 K km s $^{-1}$), C^{18}O (0.2–0.7 by 0.1 K km s $^{-1}$), and 850 μm dust continuum emission (10–70 by 10 mJy beam $^{-1}$). Molecular data, with an angular resolution of $\sim 25''$, are from Bergin et al. (2002) and dust emission (angular resolution of 14.5'') from Bianchi et al. (2003).

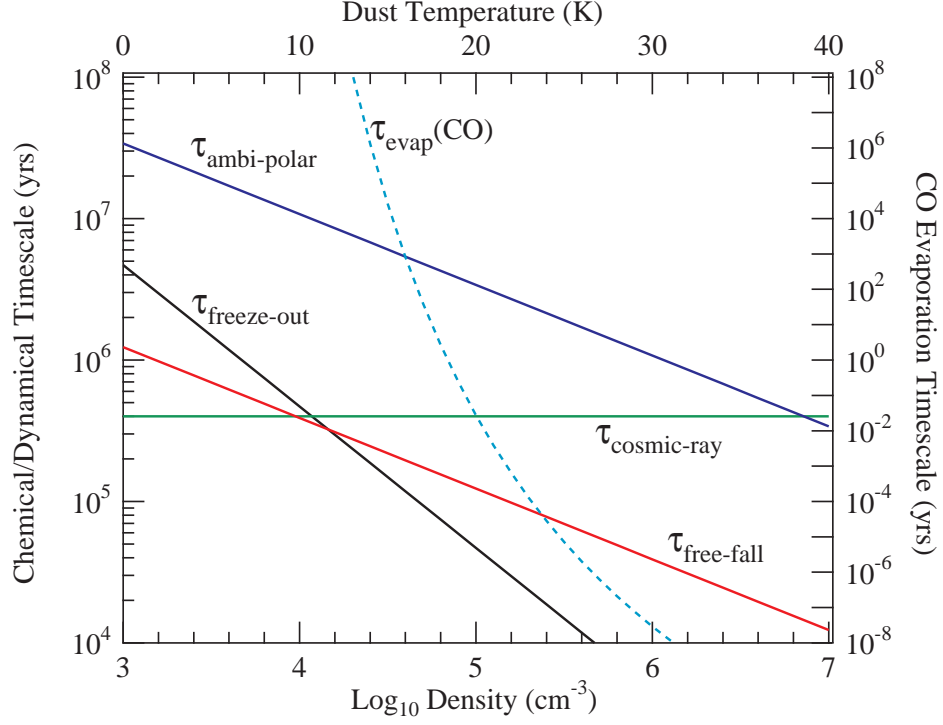


Figure 8: Plot of various chemical and dynamical timescales shown as a function of the molecular hydrogen volume density. Also shown is the density independent CO evaporation timescale as function of the dust temperature (which in the plot is also not a function of the density). Relevant equations for each quantity are provided in § 4.3.2 and § 4.4.2. In this plot the cosmic ray timescale is set by the time for any change from an equilibrium state to be reset by cosmic ray powered chemistry. The ambipolar diffusion term assumes $x_e = 2 \times 10^{-8} (n_{H_2}/10^5 \text{ cm}^{-3})^{-0.5}$.

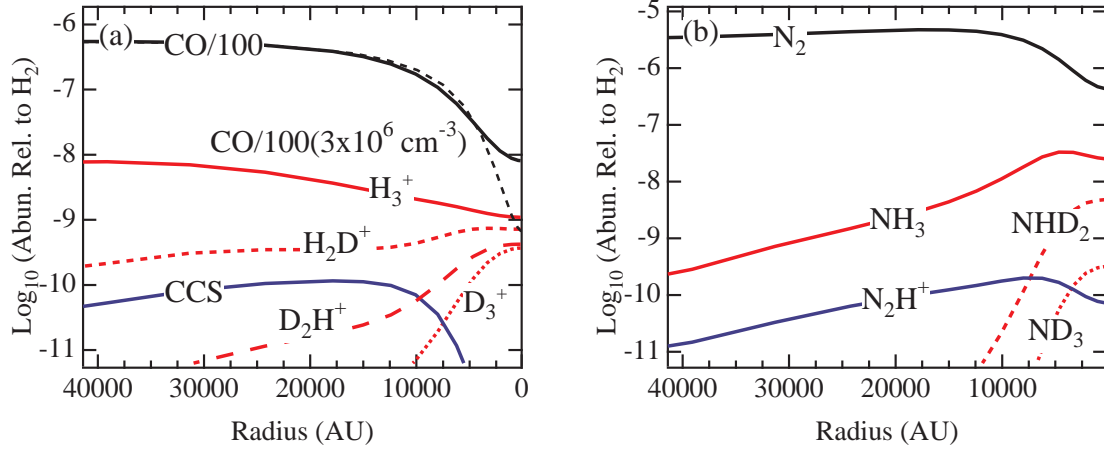


Figure 9: Plot of chemical abundances as a function of core depth for selected species from a chemical and dynamical model of a contracting Bonnor-Ebert sphere (taken from Aikawa et al. 2005). All species are shown at a timescale where $n_H(\text{center}) = 3 \times 10^5 \text{ cm}^{-3}$, excluding CO which also is shown at $n_H(\text{center}) = 3 \times 10^6 \text{ cm}^{-3}$.

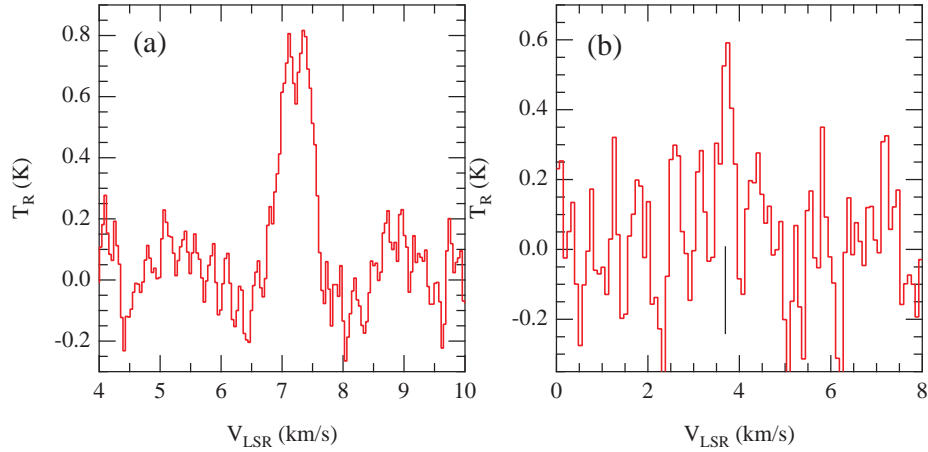


Figure 10: (a) Detection of H_2D^+ emission in L1544 (Caselli et al. 2003; van der Tak et al. 2005). (b) 4.4σ detection of D_2H^+ in the starless core IRAS16293e (Vastel et al. 2004).

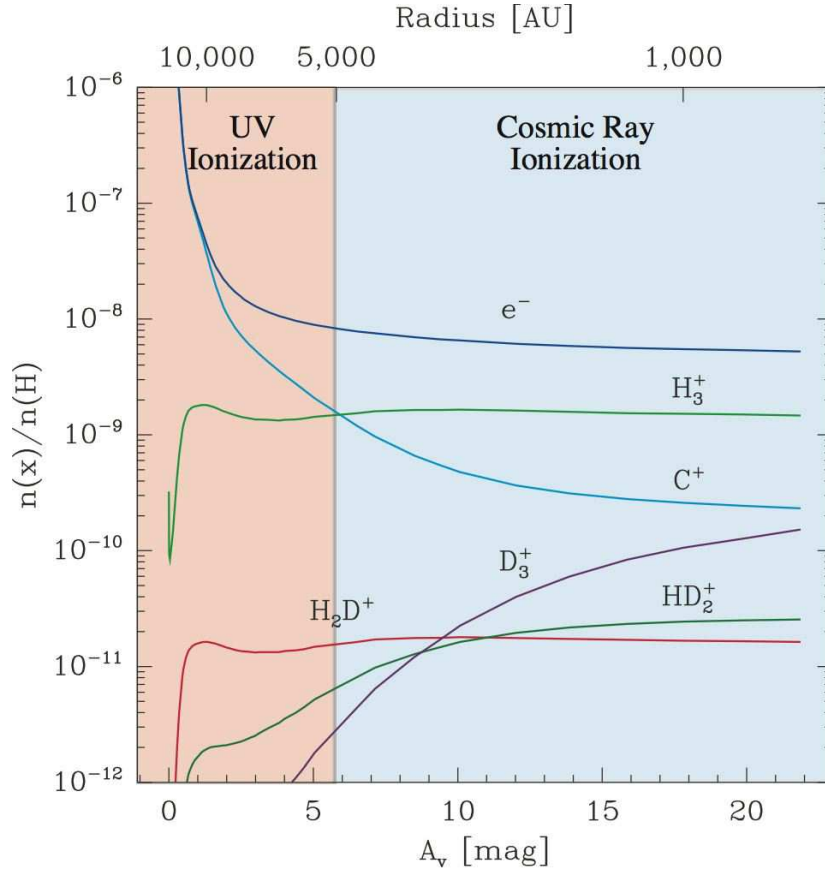


Figure 11: Derived electron fraction and major ion abundances in the Barnard 68 core. Abundances are relative to H nuclei. Zones where the ionization is dominated by UV and Cosmic Ray are delineated (effectively where C^+ is no longer the most abundant ion). In this plot H_3^+ is the main ion, carrying $\sim 20\%$ of the charge with the remainder contained in more complex ions. Taken from Maret & Bergin (2007), in prep. Some uncertainties in these calculations include the gas-grain model (i.e. the assumed binding strengths and desorption mechanisms) and the cosmic-ray ionization rate.

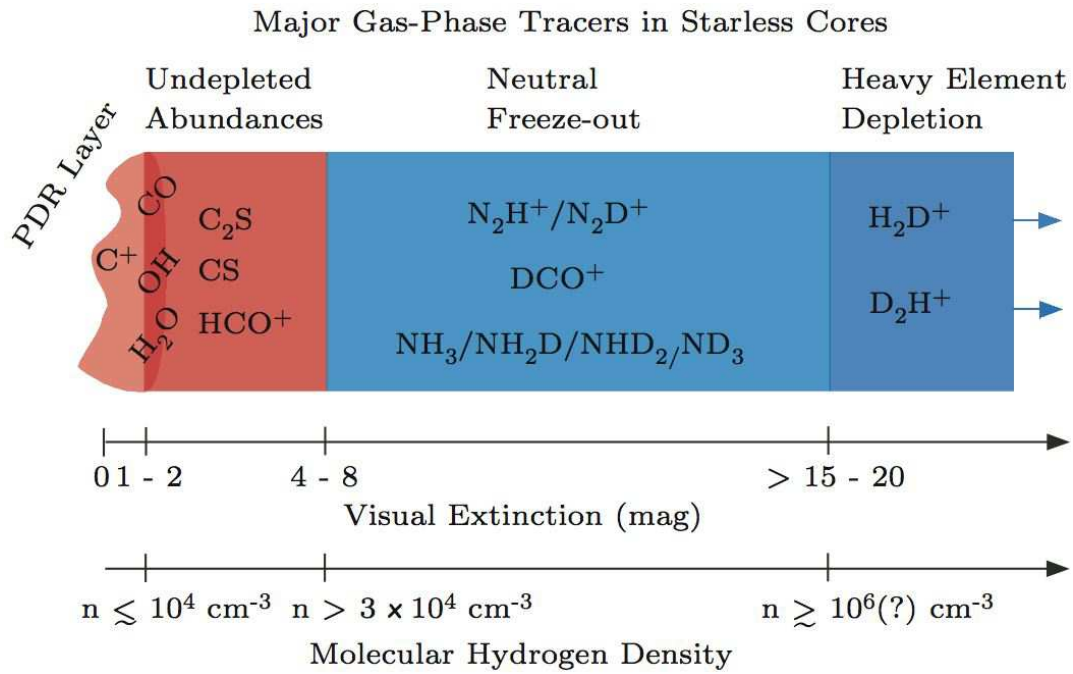


Figure 12: Schematic summary of the major gas-phase probes of starless cores as a function of depth and density. The scales provided are approximate and were estimated from Barnard 68. In this schematic the temperature is assumed to be low (< 15 K) below $A_V \sim 2$ mag.

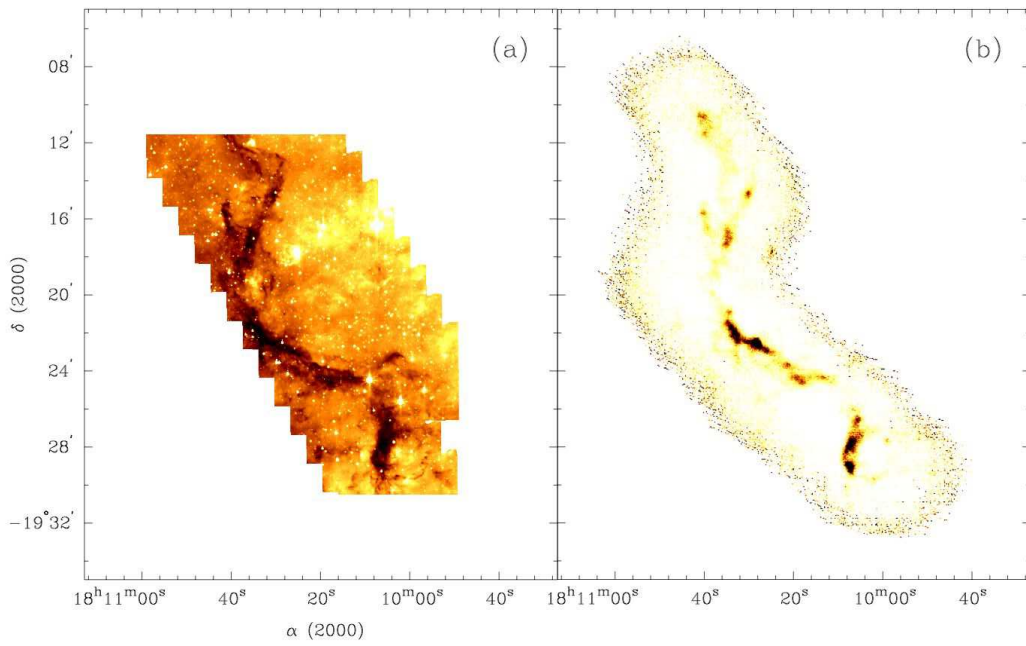


Figure 13: G11.11-0.12 infrared dark cloud as seen by (a) Spitzer IRAC band 4 and (b) $850\ \mu\text{m}$ submillimeter continuum emission (Johnstone et al. 2003). In the Spitzer image the bright infrared background is provided by PAH emission within the $8\mu\text{m}$ band and the cloud appears in absorption. In contrast, the submm continuum emission highlights the dense regions seen in absorption in the mid-infrared.